ER Stress Sensor PERK Promotes T-cell Pathogenicity in GVHD by Regulating ER-Associated Degradation

Qiao Cheng[1], Hee-Jin Choi[1], Yongxia Wu[1,2], Xiaohong Yuan[1], Allision Pugel[1], Linlu Tian[1], Michael Hendrix[1,2], Denggang Fu[1], Reza Alimohammadi[1], Chen Liu[3], Xue-Zhong Yu[1,2,4]

[1]Department of Microbiology & Immunology, Medical College of Wisconsin, Milwaukee, WI, USA

[2]Cancer Center, Medical College of Wisconsin, Milwaukee, WI, USA

[3]Department of Pathology, Yale University, New Haven, CT, USA

[4]Department of Medicine, Medical College of Wisconsin, Milwaukee, WI, USA

Authorship note: QC and H-J C contributed equally to this work.

Conflict of interest: The authors have declared that there is no conflict.

Address corresponding to: Xue-Zhong Yu, Department of Microbiology & Immunology, Department of Medicine, the Cancer Center, Medical College of Wisconsin, Milwaukee, WI, USA. Phone: 414.955.8187; Email: xuyu@mcw.edu

Abstract

Endoplasmic reticulum (ER) stress through IRE1/XBP-1 is implicated in the onset and progression of graft-versus-host disease (GVHD), but the role of ER stress sensor PERK in T-cell allogeneic responses and GVHD remains unexplored. Here, we report that PERK is a key regulator in T-cell allogeneic response and GVHD induction. PERK augments GVHD through increasing Th1 and Th17 population, while reducing Treg differentiation by activating Nrf2 pathway. Genetical deletion or selective inhibition of PERK pharmacologically reduces GVHD while preserving graft-versus-leukemia (GVL) activity. At cellular level, PERK positively regulates $CD4^+$ T-cell pathogenicity, while negatively regulating $CD8^+$ T-cell pathogenicity in the induction of GVHD. At molecular level, PERK interacts with SEL1L and regulates SEL1L expression, leading to augmented T-cell allogeneic responses and GVHD development. *In vivo*, PERK deficiency in donor T cells alleviate GVHD through ER-associated degradation (ERAD). Furthermore, pharmacological inhibition of PERK with AMG44 significantly suppresses the severity of GVHD induced by murine or human T cells. In summary, our findings validate PERK as a potential therapeutic target for the prevention of GVHD while preserving GVL responses, and uncover the mechanism by which PERK differentially regulates $CD4^+$ *versus* $CD8^+$ T-cell allogeneic and anti-tumor responses.

Introduction

Acute graft-versus-host disease (GVHD) is a major complication that leads to the morbidity or mortality of patients with hematological malignancies receiving allogeneic hematopoietic cell transplantation (allo-HCT) (1, 2). GVHD is characterized with excessive activation of donor T cells and high levels of inflammatory cytokines. Endoplasmic reticulum (ER) stress through IRE1/XBP-1 pathway has been reported to increase upon GVHD onset, correlating with the severity of GVHD (3). While ER stress is an emerging regulator in GVHD development (4), the role of ER stress sensor PERK in T-cell allogenic responses and GVHD pathogenicity is not clear.

An accumulation of unfolded or misfolded proteins in the ER leads to ER stress response. Activation of unfolded protein responses (UPR) controls the quality of the proteome pool in ER stressed cells and maintains the intracellular protein homeostasis (5). UPR is involved in the development and effector function of diverse immune cells, including T cells (6-8), dendritic cells (DCs) (9-11), macrophages (12), and myeloid cell-driven immunosuppressive cells (MDSCs) (13). Thus, targeting UPR is becoming a promising strategy in managing human diseases (14, 15). The UPR signaling includes three primary regulators: inositol-requiring enzyme-1α (IRE-1α), activating transcription factor-6 (ATF-6), and protein kinase R-like endoplasmic reticulum kinase (PERK), encoded by Eif2ak3 (16). Recently, IRE1α-mediated X-box binding protein (XBP1) signaling was reported to promote GVHD (9, 17), but the mechanism of how the ER stress sensors, PERK and XBP1, regulate T-cell allogeneic response and GVHD induction is essentially uncharacterized.

PERK resides in the ER lumen and includes 3 domains, luminal domain, transmembrane domain, and cytosolic domain (18, 19). C/EBP homologous protein (CHOP) induced by ER stress was reported to suppress anti-tumor $CD8^+$ T cell immunity through inducing ATF4 and directly repressing T-bet expression, a master regulator of T-cell effector function (20). Inhibition of PERK promotes anti-tumor immunity through suppressing immunosuppressive capacity of macrophages (12). Tumor driven PERK was reported to promote immune evasion through regulating

SEC61β-induced paraptosis and type I interferons (7). However, the function of PERK regulating $CD4^+$ T cells is not thoroughly described. ER-associated protein degradation (ERAD) is a cellular pathway that targets misfolded proteins of ER for ubiquitination and subsequent degradation via proteasome (21). SEL1L-HRD1 axis as a key component of ERAD signaling pathway was reported to be involved in Th1/Th17 differentiation in EAE mice (22). In addition, SEL1L has been reported to control the survival of $CD8^+$ T cells (23) and is required for the function and memory formation of $CD8^+$ T cells (24). However, the role of SEL1L in T-cell allogeneic response and GVHD induction has not been elucidated.

In current study, we observed that genetic ablation of PERK reduced T-cell allogeneic responses and GVHD induction, while promoting T-cell antitumor immunity. Thus, PERK appears to play a distinct role in regulating T-cell allogeneic *versus.* (*vs.*) antitumor response. Our findings provide evidence that PERK can serve as a potential therapeutic target for the prevention of GVHD while preserving GVL responses. The study also elucidates the mechanism by which PERK distinctly regulates $CD4^+$ *vs.* $CD8^+$ T-cell allogeneic and antitumor responses.

Results

*Allogeneic stimulation activates ER stress signaling in T cells***.** To investigate whether ER stress is involved in allogeneic T-cell response, we established syngeneic and murine allogeneic bone marrow transplantation (BMT) models (Figure 1A), T cell allogeneic responses were increased in the recipients after allo-BMT (Supplemental Figure 1, A-C), and we found that *Eif2ak3* (encoding PERK), *Syvn1*, *Sel1l*, *Erlec1*, *Atf4*, *Chop* were significantly increased in the T cells after allogeneic response (Figure 1B). *In vitro*, we verified that phosphate-PERK (p-PERK) and XBP-1s increased significantly in $CD4^+$ and $CD8^+$ T cells after allogeneic stimulation (Supplemental Figure 1, D-E). These data suggest that ER stress signaling may play an essential role in allogeneic T-cell response.

PERK promotes allogeneic responses of $CD4^+$ T cells and exacerbates GVHD. To

further evaluate how PERK and XBP1 affect T-cell response to alloantigen *in vivo*, we utilized cKO mice on B6 background that are specifically deficient for PERK or XBP1 in their T cells, respectively (Supplemental Figure 2A). To assess whether PERK or XBP1 impacts T-cell development, we analyzed the frequency of both $CD4^+$ and $CD8^+$ T cells, $CD44^+CD62L^-$ (effector memory), $CD44^+CD62L^+$ (central memory), and $CD44^-CD62L^+$ (naïve) in PERK or XBP1 cKO mice. There was no significant difference in the percentages of $CD4^+$ and $CD8^+$ T cells in PERK or XBP1-deficient mice compared with wild type (WT) mice (Supplemental Figure 2, B-D). We further demonstrated that PERK or XBP1 deficiency did not significantly affect the percentages of naïve, effector memory, or central memory $CD4^+$ T and $CD8^+$ T cells when compared with WT mice (Supplemental Figure 2, E-G). Thus, both PERK and XBP1 do not affect the development of T cells or their phenotypes at homeostatic condition.

To determine whether PERK regulates T-cell allogeneic responses, T cells isolated from WT and PERK cKO mice were labeled with CFSE, and then co-cultured with T cell-depleted splenocytes (TCD-SP) as allogeneic APCs. PERK deficiency markedly reduced the proliferation and activation of $CD4^+$ but not $CD8^+$ T cells as reflected by lower percentage of $CFSE^{low}$ cells and reduced TNFα levels (Figure 1, C-E). Therefore, PERK preferentially promotes allogeneic responses of $CD4^+$ T cells *in vitro*.

To assess whether PERK or XBP1 regulates T-cell-driven GVHD, we used an MHC-mismatched murine BMT model, B6 → BALB/c. As compared with WT T cells, PERK-deficient T cells induced significantly milder GVHD in allogeneic recipients reflected by better survival (Figure 1F), reduced clinical scores (Figure 1G) and body weight loss (Figure 1H). However, XBP1-deficient T cells induced severe GVHD similarly as WT T cells (Figure 1, F-H). Consistently, the recipients of PERK-deficient donor T cells had significantly improved thymocyte recovery and B-cell reconstitution as compared with those of WT or XBP1-deficient T cells (Supplemental Figure 3, A-B). Taken together, PERK promotes T-cell pathogenicity in the induction of GVHD in mice.

PERK deficiency in donor T cells alleviates gut GVHD through reducing Th1, Th17 subsets and increasing Treg generation. To explore how PERK regulates T-cell-

mediated GVHD, we used the same allogeneic BMT model (B6 → BALB/c) as described above. PERK-deficient T cells induced milder GVHD reflected by less body weight loss of the recipients when compared with WT T cells, which is consistent with long-term BMT experiments (Supplemental Figure 4, A-B). Two weeks after BMT, pathologic analyses confirmed that the recipients of PERK-deficient T cells had significantly reduced injuries in the liver, as well as the small and large intestines as compared with those of WT or XBP1-deficient T cells (Figure 2, A-B). We examined donor T cells in recipient intestines and found that infiltrated $CD4^+$ and $CD8^+$ T cells were decreased in recipients receiving PERK-deficient T cells as compared with those in the recipients of WT XBP1-deficient T cells (Figure 2C). We further observed that only PERK- deficient T cells significantly reduced CXCR3 expression levels on donor $CD4^+$ and $CD8^+$ T cells. PERK deficiency also significantly reduced IFNγ and substantially decreased IL-17 production by donor $CD4^+$ but not $CD8^+$ T cells (Figure 2, D-F). We also observed that PERK deficiency significantly decreased CXCR3, TNFα, IL-17A in donor $CD4^+$ but not $CD8^+$ T cells in recipient small intestine (Supplemental Figure 4, C-E). Based on these findings, PERK may promote allogeneic T-cell differentiation towards Th1 and Th17 cells that are major pathogenic subsets for GVHD induction.

In addition, we found that the frequency and absolute number of $CD4^+Foxp3^+$ T cells were increased among PERK-deficient T cells as compared with WT or XBP1-deficient counterparts (Supplemental Figure 5, A-C). Consistently, PERK deficiency promoted T-cell differentiation towards $CD25^+Foxp3^+$ Tregs under Treg-polarization condition *in vitro* (Supplemental Figure 5, D-E). Nrf2 is known to be a key regulator for Treg differentiation(25). We therefore analyzed the levels of Nrf2 in Treg cells and found that PERK deficiency significantly reduced the levels of Nrf2 (Supplemental Figure 5F). To further assess whether PERK regulated Treg differentiation through Nrf2, we activated Nrf2 using sulforaphane (SFN) and observed that SFN treatment reversed the heightened Treg-differentiation as well as Helios expression due to PERK deficiency (Supplemental Figure 5, G-I). Thus, PERK appears to regulate Treg differentiation through Nrf2 signaling pathway.

PERK deficiency or inhibition does not impact T-cell-mediated GVL effect. The data presented so far indicate that PERK but not XBP1 impacts T-cell allogeneic response and GVHD induction, and we thus focused the rest of the study on PERK. Because allo-HCT is primarily applied as a therapeutic approach to treat hematological malignancies, such as leukemia, we wanted to evaluate the impact of PERK on T-cell mediated GVL activity. For this end, CD25-depleted T cells isolated from WT and PERK cKO mice were injected into BDF1 mice along with luciferase-transduced host-type mastercytoma (P815) cells. Consistently, the recipients of PERK-deficient T cells had milder GVHD than those of WT T cells reflected by improved survival and decreased clinical scores (Figure 3, A-B). Furthermore, pathologic analyses confirmed that the recipients of PERK-deficient T cells had significantly reduced injuries in the liver, lung, and small intestines when compared with those of WT T cells (Supplemental Figure 6, A-B). More importantly, PERK deficiency in T cells preserved GVL activity in this haploidentical BMT model (Figure 3C). In addition, PERK-deficient donor T cells exhibited intact GVL activity against mixed lineage leukemia (MLL) but induced milder GVHD reflected by prolonged survival in recipients after MHC-mismatched BMT (Supplemental Figure 7, A-D). These results indicate that PERK deficiency preserves GVL affect while reducing GVHD.

For translational purposes, we next evaluated the effect of ER stress inhibition in allogeneic response *in vitro* by testing an ER stress inhibitor (tauroursodeoxycholic acid, TUDCA). TUDCA is a naturally occurring hydrophilic bile acid, which has been shown to attenuate ER stress, prevent unfolded protein response dysfunction, and stabilize mitochondria (26). TUDCA is FDA-approved for treating biliary cirrhosis. Recent studies show that TUDCA has additional beneficial effects in neurodegenerative diseases (27), osteoarthritis (28), vascular diseases (29), and diabetes (30). We first tested the effect of TUDCA in T-cell responses *in vitro*. Consistent with the genetic model, we observed that TUDCA significantly decreased $CD4^+$ T-cell proliferation (CFSE dilution) and activation (IFNγ production) upon allogeneic stimulation *in vitro* (Supplemental Figure 8A). Furthermore, TUDCA treatment significantly prolonged recipient survival (Figure 8B) and reduced clinical scores (Supplemental Figure 8C).

Consistent with PERK-deficiency in T cells, TUDCA treatment also preserved the GVL activity (Supplemental Figure 8D). Given TUDCA inhibits both PERK and XBP1, we attempted to determine how much the contribution of TUDCA treatment to GVHD alleviation was due to inhibition of XBP1 *vs.* PERK. To do so, we transplanted XBP1-deficienct T cells and treated the recipients with TUDCA. As shown in Figure 1, F-H, XBP1-deficient T cells induced similarly severe GVHD as WT cells. The treatment with TUDCA was effective in preventing GVHD while preserving the GVL activity induced by either type of T cells (Supplemental Figure 8, E-G). Taken together, these findings suggest that targeting ER stress by TUDCA can preserve GVL activity while attenuating GVHD primarily through inhibiting PERK.

AMG44 is a highly selective PERK inhibitor with an IC50 of 6 nM that has been tested in several recent studies (20, 31, 32). We therefore tested AMG44 and found that the PERK specific inhibitor significantly reduced proliferation and IFNγ production of $CD4^+$ T cells in response to alloantigen stimulation *in vitro* (Figure 3D). Furthermore, treatment with AMG44 significantly attenuated GVHD severity (Figure 3, E-G) while preserving the GVL effect (Figure 3H). Thus, our data indicate PERK serving as a potential therapeutic target for the prevention of GVHD while maintaining GVL activity after allogeneic BMT.

PERK differentially regulates $CD4^+$ and $CD8^+$ T-cell allogeneic responses. To explore how PERK regulates T-cell allogeneic responses, $CD4^+$ or $CD8^+$ T cells were isolated from WT or PERK cKO mice and stimulated separately with allo-APCs from BDF1 mice *in vitro*. We found that PERK deficiency reduced the proliferation and cytokine secretion of $CD4^+$ T cells after allogeneic stimulation (Figure 4, A-B). In contrast, PERK deficiency promoted the proliferation and cytokine secretion of $CD8^+$ T cells (Figure 4, C-D). These results suggest that PERK differentially regulates the allogeneic responses of $CD4^+$ and $CD8^+$ T cells *in vitro*. To determine whether PERK would regulate $CD4^+$ and $CD8^+$ T-cell allo-responses *in vivo*, $CD4^+$ or $CD8^+$ T cells were isolated from WT or PERK cKO mice and transferred into lethally irradiated BALB/c mice separately. PERK-deficient $CD4^+$ T cells showed reduced ability to induce GVHD

(Figure 4, E-G). In sharp contrast, PERK-deficient $CD8^+$ T cells had increased ability to cause GVHD (Figure 4, H-J). Consistent with GVHD pathogenicity, PERK-deficient $CD8^+$ T cells were found to produce higher levels of IFNγ, TNFα and GM-CSF in allogeneic recipients (Supplemental Figure 9, A-B). Taken together, PERK distinctly regulates $CD4^+$ and $CD8^+$ T cell allogeneic responses.

To further investigate whether the effects of AMG44 on T-cell allogenic responses depend on PERK expression of T cells. We found that AMG44 treatment significantly inhibited the proliferation or cytokine productions of WT $CD4^+$ T cells after allo-stimulation but not PERK cKO $CD4^+$ T cells (Supplemental Figure 10, A-B), suggesting the specificity of AMG44 in the inhibition of PERK. AMG44 treatment did not significantly reduce the proliferation and cytokines in PERK-deficient $CD8^+$ T cells as compared with vehicle-treated PERK-deficient $CD8^+$ T cells (Supplemental Figure 10, C-D). To evaluate the specificity of AMG44 *in vivo*, we transplanted WT or PERK cKO CD8 T cells into allogeneic recipients and treated them with AMG44. AMG44 treatment promoted GVHD induced by WT $CD8^+$ T cells (Supplemental Figure, 10 E-F), which mimics genetic PERK deficiency (Figure 4, H-J). However, AMG44 treatment ameliorated GVHD severity induced by PERK-deficient $CD8^+$ T cells (Supplemental Figure, 10 E-F), suggesting that PERK inhibition could suppress CD4-helper function or non-T cells such as APCs.

PERK inhibits $CD8^+$ T-cell responses. We further investigated how PERK regulates $CD8^+$ T-cell responses, which may contribute to the preserved GVL effect when PERK was deficient or inhibited. $CD8^+$ T cells were purified from 2C TCR Tg WT or PERK cKO mice and stimulated with allo-APCs or SIYRYYGL (SIY) peptide. As compared with WT 2C T cells, PERK-deficient 2C T cells showed increased activation, reflected by higher IFNγ and TNFα production, in response to alloantigens (Figure 5, A-B) as well as peptide antigen *in vitro* (Figure 5, C-D). These results suggest that PERK restricts $CD8^+$ T-cell responses *in vitro*. To further investigate the role PERK in donor $CD8^+$ T-cell mediated GVH/GVL responses *in vivo*, $CD8^+$ T cells were isolated from 2C TCR Tg WT or PERK cKO mice and transferred into lethally irradiated BDF1 mice.

To facilitate $CD8^+$ T-cell response *in vivo*, a small number of $CD4^+$ T cells from normal B6 mice were co-transferred with 2C T cells as $CD8^+$ 2C T cells alone can only induce mild GVHD limited to hematopoietic compartment (33). We then observed that PERK-deficient 2C T cells were trending higher pathogenesis of GVHD (Figure 5, E-F) while maintaining a strong GVL effect (Figure 5G). To investigate the role of PERK more specifically in antitumor response of $CD8^+$ T cells, we stimulated pMEL TCR Tg cells with specific antigen gp100 *in vitro* and found that PERK-deficient $CD8^+$ T cells secreted higher levels of IFNγ and IL-17 production (Figure 5H). Furthermore, pMEL TCR Tg PERK-deficient $CD8^+$ T cells prolonged the survival of mice bearing B16F10 melanoma (Figure 5, I-J). Taken together, these results indicate that PERK deficiency promotes $CD8^+$ T cell responses.

PERK distinctly regulates T-cell responses to allogeneic vs. polyclonal stimulation. To explore potential mechanisms by which PERK regulates $CD4^+$ and $CD8^+$ T-cell responses, we examined the role of PERK in T-cell responses after stimulation with allogeneic APCs or anti-CD3/CD28. In gated $CD4^+$ T cells, PERK-deficiency reduced the production of IFNγ and GM-CSF upon allogeneic stimulation, but increased cytokine production upon polyclonal stimulation (Supplemental Figure 11, A-C). In gated $CD8^+$ T cells, PERK-deficiency had little impact on cytokine production upon allogeneic stimulation, but increased cytokine production upon polyclonal stimulation (data not shown). Thus, PERK appeared to distinctly regulate T-cell allogeneic and polyclonal responses, especially $CD4^+$ T cells. Cao *et al.* reported that PERK deficiency promotes T-cell activation and antitumor response by decreasing *Ddlt3* mRNA (encoding CHOP) and CHOP protein while increasing T-bet expression (20). To determine how PERK differentially regulates T cell response to polyclonal *vs.* allogeneic stimulation, we measured Ddlt3, CHOP and T-bet levels after T-cell stimulation. Consistent with the observations by Cao *et al.,* we found that PERK-deficient T cells, both $CD4^+$ and $CD8^+$, decreased Ddlt3 and CHOP expression while increasing T-bet expression after polyclonal stimulation (Supplemental Figure 11, D-G). In sharp contrast, PERK-deficient T cells increased Ddlt3 and CHOP expression while decreasing T-bet expression after allogeneic stimulation, especially in $CD4^+$ T

cells (Supplemental Figure 11, D-G).

To investigate how PERK regulates T-cell response in polyclonal *vs*. allogeneic stimulation at the metabolic level, we found that mitochondrial content was significantly reduced in PERK-deficient $CD4^+$ but not $CD8^+$ T cells after allogeneic stimulation (Supplemental Figure 11, H-I). In contrast, mitochondrial content was significantly increased in PERK-deficient $CD4^+$ and $CD8^+$ T cells after polyclonal stimulation (Supplemental Figure 11, H-I). We then measured T-cell metabolism by Seahorse analysis. In the absence of PERK, T cells reduced oxidative phosphorylation, as reflected by oxygen consumption rate (OCR), upon allogeneic stimulation, whereas T cells had a similar level of oxidative phosphorylation upon polyclonal stimulation regardless of PERK expression (Supplemental Figure 11, J-K). Similarly, PERK-deficient T cells significantly reduced glycolysis reflected by extracellular acidification rate (ECAR) upon allogeneic stimulation, whereas these T cells significantly increased glycolysis upon polyclonal stimulation (Supplemental Figure 11, L-M). These results suggest that PERK differentially regulates T-cell OXPHOS and glycolysis upon polyclonal *vs*. allogeneic stimulation.

PERK regulates T-cell allogeneic responses through ERAD signaling. To further elucidate the mechanism of PERK differentially regulating T cell allogeneic and anti-tumor responses, we performed transcriptomics analyses via bulk RNA sequencing on WT and PERK-deficient T cells after allogeneic and polyclonal stimulation. All the differentially expressed genes in PERK-deficient vs. WT T cells after allogeneic and polyclonal stimulation were presented in the volcano plots (Supplemental Figure 12). The transcriptomics data showed that ERAD-associated genes, including Sel1l and Erlec1, were significantly increased in PERK cKO compared with WT T cells upon allogeneic but not polyclonal stimulation (Figure 6A). Increased mRNA levels of ERAD-associated genes were confirmed with qPCR in PERK-cKO T cells upon allogeneic stimulation (Figure 6B). Consistently, protein levels of SEL1L and ERLEC1 were also increased in allogeneic PERK-deficient T cells (Figure 6C). When stimulated with alloantigen separately, PERK-deficient $CD4^+$ and $CD8^+$ T cells upregulated SEL1L

(Supplemental Figure 13A) and thus decreased amyloid β-protein aggregation (Supplemental Figure 13, B-C). However, SEL1L protein levels were decreased in PERK-deficient $CD8^+$ T cells after polyclonal stimulation (Supplemental Figure 13D) with increased accumulation of aggregates (Supplemental Figure 13E). In addition, protein levels of CHOP were increased in PERK-deficient $CD4^+$ T cells but not $CD8^+$ T cells after allogeneic stimulation (Supplemental Figure 13F). In contrast, CHOP protein levels were markedly decreased in PERK-deficient $CD8^+$ T cells after polyclonal stimulation (Supplemental Figure 13G), which is consistent with reported data (20). To determine whether PERK regulates T cell allogeneic responses through regulating ERAD pathway, we stimulated T cells with allogeneic APCs or anti-CD3/CD28 in the presence of kifunensine, an ERAD inhibitor (34). Kifunensine reversed the defect of PERK-deficient $CD4^+$ T cells in IFNγ production upon allogeneic stimulation (Supplemental Figure 14, A-B), but not upon polyclonal stimulation (data not shown). Furthermore, Kifunensine also reversed the reduced mitochondria components and elevated CHOP levels in PERK-deficient $CD4^+$ T cells after alloantigen stimulation (Supplemental Figure 14, C-D). These data support that the elevated ERAD contributes to the impaired allogeneic T-cell responses in the absence of PERK.

Because SEL1L-HRD1 axis plays a central role in ERAD pathway (35), we determined to test whether PERK interacts with SEL1L. Indeed, we observed that PERK binds to SEL1L in activated human T-cell line (Supplemental Figure, 15A). To verify whether PERK regulates T-cell allogeneic responses dependent on SEL1L-mediated ERAD pathway, we generated SEL1L and PERK dKO mice, and demonstrated that additional SEL1L deficiency reversed the defects of PERK cKO $CD4^+$ T cells in response to alloantigen, reflected by mitochondrial components, proliferation and TNFα production *in vitro* (Supplemental Figure 15, B-E). Moreover, SEL1L deficiency largely reversed the reduced ability of PERK cKO T cells in the induction of GVHD (Figure 6, D-F). Consistent with in *vitro* studies, we found that PERK cKO did not reduce cytokine productions (Figure 6, G-I) or increase CHOP expression (Figure 6, J-K) when SEL1L was absent as well. These results elucidate that PERK regulates T-cell allogeneic

responses and GVHD induction through SEL1L-mediated ERAD pathway.

Pharmacological inhibition of PERK reduces GVHD induced by human T cells while increasing GVL activity. To promote translation, we next investigated the role of PERK in human T-cell responses. T cells were isolated from human PBMCs, labeled with CFSE, and stimulated with allogeneic APCs (TCD-PBMCs) with or without AMG44. We observed that AMG44 supplement suppressed proliferation, reduced IFNγ, TNFα production by $CD4^+$ T cells in response to allogeneic stimulation, but did not impact proliferation and TNFα production of $CD8^+$ T cells while slightly decreasing IFNγ production (Figure 7, A-C). Consistent with mouse data, AMG44 promoted IFNγ and TNFα in $CD4^+$ and $CD8^+$ T cells stimulated with anti-CD3/CD28 (Supplemental Figure 16, A-C). We then conducted an *in vivo* study using a xenograft GVHD model and found that AMG44 treatment reduced GVHD induced by human T cells reflected by better GVHD survival (Figure 7D), reduced body weight loss (Figure 7E) and clinical scores (Figure 7F). More importantly, AMG44 also preserved GVL activity (Figure 7G). These results indicate that PERK inhibition can preserve GVL effects while attenuating GVHD induced by human T cells.

Discussion

The present study demonstrates that targeting ER stress sensor PERK suppresses GVHD while preserving the GVL activity. PERK promotes CD4 T-cell differentiation towards Th1 and Th17 subsets while limiting their differentiation into Treg subset. On the other hand, PERK negatively regulates $CD8^+$ T cell-mediated allogeneic responses and antitumor responses. Thus, PERK differentially regulates $CD4^+$ and $CD8^+$ T cell allogeneic responses. This study provides evidence that PERK is a promising ER stress target to reduce GVHD while maintaining GVL effect.

Our findings reveal that PERK promotes the proliferation and pro-inflammatory cytokines in allogeneic $CD4^+$ T cells, thereby exacerbating GVHD; On the other hand, PERK inhibits the proliferation and pro-inflammatory cytokines in allogeneic $CD8^+$ T cells that may contribute to the preserved GVL effect. When total T cells were

transferred into allogeneic recipients, PERK cKO T cells significantly reduced their ability to include GVHD while preserving the GVL effect (Figure 1-3, 6). Similarly, the recipients treated with PERK inhibitor significantly reduced GVHD while sparing GVL activity (Figure 3, 7). Under the condition where $CD8^+$ T cells deficient for PERK increased allogeneic response, CD4 helper was provided by WT $CD4^+$ T cells (Figure 4, 5). We interpret that, when PERK is deficient or blocked, $CD4^+$ T cells are incapable of providing a strong helper to CD8 T cells, and therefore $CD8^+$ T cells even lacking PERK cannot mount a powerful allogeneic response to induce severe GVHD while mediating an adequate GVL response. Taking these results together, we reason that inhibition of PERK can be translated to the clinic for controlling GVHD and leukemia relapse after allogeneic HCT.

The activating effects of PERK on $CD4^+$ T cells in allogeneic responses are consistent throughout the study. However, the effect of PERK on $CD8^+$ T cells appears to be somewhat inconsistent, and we interpret the data in several folds as the following: 1) when total T cells were stimulated with alloantigen, the degree of CD4 helper influences CD8 responses. Under this condition, we observed that, in the absence of PERK on both types of T cells, CD8 T-cell response was not increased (Figure 2C-D, Supplemental Figure 4C-E and 11G, I). However, when purified CD8 T cells were stimulated alone without CD4 helper *in vitro*, the suppressive effects of PERK on CD8 T cells become apparent (Figure 4A-D and 5A-D). Under *in vivo* condition, the suppressive effects of PERK on CD8 T cells were also obvious (Figure 4F-J and 5E-G, Supplemental Figure 10C-D), which was likely due to a strong helper provided by additional WT CD4 T cells. 2) In terms of human T cells, CD8 T-cell response was slightly decreased when PERK was inhibited by AMG44 (Figure 7A-C). It is likely that impaired CD4 helper function impacted CD8 T-cell response. The interpretation is supported by the observation that the response of human CD8 T cells was significantly increased when T cells were activated by strong poly-clonal stimulation *in vitro* (Supplemental Figure 16). One other possibility is that, unlike T-cell specific PERK deficiency (Figure 4 and 5), the PERK inhibition could impact APCs as well (36). 3) most importantly, pharmacological inhibition of PERK significantly reduced GVHD

while preserving the GVL effect in vivo regardless of experimental models, which set a strong rationale for clinical translation.

CHOP as PERK downstream target was reported to impair the effector function of tumor-infiltrating T cells in murine tumor models. In ovarian cancer patients, increased expression of CHOP in tumor infiltrating $CD8^+$ T cells was associated with poor clinical outcome (20). In current study, when $CD4^+$ or $CD8^+$ T cells were stimulated separately, we found that PERK deficiency increases CHOP levels in $CD4^+$ T cells, but not in $CD8^+$ T cells after allogeneic stimulation (Supplemental Figure 9F). CHOP levels were decreased in PERK-deficient $CD8^+$ T cells upon polyclonal stimulation (Supplemental Figure 9G). The finding that PERK distinctly regulates $CD4^+$ and $CD8^+$ T-cell allogeneic response was further supported by *in vivo* studies (Figure 4, 5). However, we observed that PERK deficiency increases CHOP levels in $CD8^+$ T cells when $CD4^+$ and $CD8^+$ T cells were stimulated with alloantigen together *in vitro* (Supplemental Figure 8, D-E). We interpret that the upregulation of CHOP in PERK-deficient $CD8^+$ T cells was impacted by reduced helper from PERK-deficient $CD4^+$ T cells in the mixed culture. CHOP was reported to directly repress the expression of T-bet in $CD8^+$ T cells (20). Consistently, we found that PERK suppresses T-bet levels in $CD8^+$ and $CD4^+$ T cells after polyclonal stimulation (Supplemental Figure 8, F-G). Thus, distinct regulation of $CD4^+$ *vs*. $CD8^+$ T-cell allogeneic response by PERK may be at least partially through controlling CHOP expression levels.

Abrogating PERK activity in T cells was shown to resulted in decreased mitochondrial reactive oxygen species (ROS) and enhanced antitumor immunity *in vivo* (37). Additionally, PERK was reported to regulate mitochondrial biology during ER stress (38). Whether PERK affects the metabolism of allogeneic T cells or how it affects them is essentially uncharacterized. In our study, we found that PERK deletion reduces the maximal respiration and glycolysis in allogeneic T cells while promoting glycolysis in T cells after polyclonal stimulation, indicating that PERK differentially regulates the OXPHOS and glycolysis of allogeneic T cells and antitumor T cells (Supplemental Figure 8, J-M).

SEL1L-HRD1 axis is a key component of ERAD signaling pathway (35). SEL1L-HRD1 ERAD was reported to control the identity of β cells via TGF-β signaling (39). SEL1L deficiency in T cells promotes Th1/Th17 differentiation and exacerbates EAE (22). Targeting SEL1L significantly promotes the allogeneic responses of T cells *in vitro* (data not shown), but SEL1L deficiency in donor T cells did not exacerbate GVHD *in vivo* (Figure 6, D-F). SEL1L was reported to regulate the survival and homeostasis of $CD8^+$ T cells through PERK signaling pathway (23). In GVHD model, we demonstrated that PERK interacts and regulates SEL1L, and additional SEL1L-deletion reversed the defects of PERK-cKO T-cell allogeneic response (Figure 6, D-F). Thus, we interpret that PERK impacts T-cell allogeneic responses and GVHD induction at least partially through ERAD pathway. In human, SEL1L-ERAD has been reported to be involved in children's neurodevelopmental disorders, such as developmental delay, intellectual disability, microcephaly, facial dysmorphisms, hypotonia, and/or ataxia (40). The role of SEL1L in human GVHD needs to be further investigated.

Targeting ER stress by using TUDCA can reduce GVHD while preserving GVL activity. Interestingly, TUDCA still reduces GVHD while preserving GVL activity even when XBP1 was absent in donor T cells (Supplemental Figure 6, E-G). Thus, PERK not XBP1 is a potential target for TUDCA to alleviate GVHD and preserve GVL effect. The metabolite Trimethylamine N-oxide (TMAO) induced pyroptosis in tumor cells by activating ER stress kinase PERK and thus enhanced $CD8^+$ T cell-mediated antitumor immunity in triple-negative breast cancer (41). AMG44 was reported to be a more specific inhibitor that targets PERK compared to other PERK inhibitors, such as GSK2606414 and GSK2656157 (19). In murine GVHD model, we found that AMG44 treatment significantly reduces GVHD while preserving GVL activity (Figure 3, E-H). Pharmacologically targeting PERK with AMG44 also reduces human T cell-mediated GVHD while preserving GVL activity (Figure 7, D-G). These findings proved PERK as a promising target for alleviating GVHD while preserving the GVL effect, supporting clinical investigation to validate targeting PERK as a potential therapeutic strategy in the control of GVHD and leukemia relapse.

Methods

Sex as a biological variable

Our study examined male and female animals, and similar findings are reported for both sexes.

Mice and human T cells

C57BL/6 (B6, $H2K^b$, $Ly5.2^+$ or B6, $H2K^b$, $Ly5.1^+$), BALB/c ($H2K^d$), (B6 × DBA2) F1 (B6D2F1, $H2K^{b/d}$) were purchased from the National Cancer Institute Mouse Repository (Frederick, MD). NOD/SCID/$IL2Rg^{-/-}$ (NSG, HLA-$A2^+$) and $PERK^{fl/fl}$ mice were purchased from the Jackson Laboratory (Bar Harbor, ME). $XBP1^{fl/fl}$ and $SEL1L^{fl/fl}$ strain was kindly provided by Drs. Hu(42) and Lin(43), respectively. Conditional knock-out (cKO) mice for PERK, XBP1 or SEL1L on B6 background were produced by cross-breeding $PERK^{fl/fl}$, $XBP1^{fl/fl}$, $SEL1L^{fl/fl}$ mice with CD4-Cre-expressing mice, respectively. PERK/SEL1L double KO (dKO) strain was produced by cross-breeding $PERK^{fl/fl}$ and $SEL1L^{fl/fl}$ mice with CD4-Cre^+ mice. B6 2C TCR transgenic (Tg) and PERK cKO mice were bred by crossing 2C Tg with $CD4Cre^+$ or PERK cKO mice. B6 pMEL Tg and PERK cKO mice were bred by crossing pMEL Tg mice with $CD4Cre^+$ or PERK cKO mice. Human T cells were isolated from the peripheral blood mononuclear cells (PBMCs) of healthy donors purchased from Research Blood Components, LLC.

Cell culture and Reagents

Luciferase overexpressed P815 (P815-luc) and MLL-AF9-GFP cells were kindly given by Pavan Reddy at University of Michigan and Indiana University, respectively. Luciferase overexpressed B16F10 (B16F10-luc) cells were purchased from IVIS Imaging Company, Jurkat E6.1 cells were purchased from ATCC. Luciferase overexpressed Raji (Raji-luc) cells were kindly given by Defu Zeng at the City of Hope Medical Center. P815-luc, MLL-AF9-GFP, B16F10-luc, Jurkat E6.1, Raji-luc cell lines as well as all mouse and human primary T cells were cultured in RPMI 1640 medium purchased from Gibco (Grand Island, NY) supplemented with 10% FBS (Gibco, NY), as well as penicillin/streptomycin (Corning, MA), nonessential amino acids (Corning, MA), sodium pyruvate (Corning, MA), and 2-Mercaptoethanol (Gibco, NY).

AMG44 was purchased from Tocris Bioscience (Bristol, UK). Tauroursodeoxycholic Acid (TUDCA), Kifunensine, and a small-molecule Nrf2 activator Sulforaphane (SFN) were purchased from Cayman Chemical (Ann Arbor, MI). Mitotracker green and live-dead yellow were purchased from Invitrogen (Waltham, MA).

The induction and assessment of GVHD

BALB/c recipients were exposed to 900 cGy total body irradiation (TBI) by using cesium-137 irradiator before bone marrow transplantation (BMT), and then intravenously given T cell-depleted BM (TCD-BM) cells (5×10^6/mouse) from C57BL/6 (B6) or RAG1-KO donors with or without T cells (1.25×10^6) purified from B6 donors. The recipients were monitored through body weight loss and GVHD scores twice a week. (B6 x DBA2) F1 (BDF1) recipients were exposed to 1200 cGy TBI with two split doses before BMT, and then intravenously given TCD-BM cells (5×10^6) from B6 or RAG1-KO donors with or without mastocytoma P815-luc cells (5000), along with or without CD25-depleted T cells (3×10^6) purified from spleen and lymph node cells of B6 donors. For xenograft BMT model, NSG mice were exposed to 250 cGy TBI before BMT, and then intravenously given Raji-luc cells (1×10^6), along with or without HLA-$A2^-$ human PBMCs (8×10^6). The recipients were monitored through body weight loss and GVHD scores twice a week. Tumor growth was monitored using IVIS Spectrum CT. Tumor and GVHD mortality was distinguished by bioluminescence (BLI) signal intensity and GVHD manifestation. The detailed information on T cell isolation, T cell-depleted BM cells has been described previously(44, 45).

Antibodies and Flow cytometry

Monoclonal antibodies (mAbs) specific for mouse $H2K^b$ (clone AF6-88.5), CD45.1 (clone A20), CD45.2 (clone 104), CD4 (clone RM4-5), CD8 (clone 53-6.7), B220 (clone RA3-6B2), or 2C TCR (clone 1B2) were purchased from BD Bioscience. mAbs specific for mouse $H2K^d$ (clone SF1-1.1.1), CD25 (clone pc61.5), CXCR3-biotin (clone CXCR3-173), or CD62L (clone MEL-14) were purchased from eBioscience. mAb specific for mouse CD44 (clone IM7) was from Biolegend. Biotinylated antibodies were detected using streptavidin conjugates with APC-Cy7 or PE-Cy7 purchased from BD

Bioscience. mAbs specific for mouse IFNγ (clone XMG1.2), TNFα (clone MP6-XT22), GM-CSF (clone MP1-22E9), or IL-17A (clone TC11-18H10.1) were from Biolegend. mAb specific for Ki67 (clone B56), Foxp3 (cone FJK-16S), Hellios (clone 22F6), or T-bet (clone 4B10) were from BD Bioscience. Antibody against CHOP (clone B-3) was from Santa Cruz. Antibodies against phosphate PERK (p-PERK, 3179S) or XBP-1s (12782S) were from Cell Signaling Technology. Antibody against Nrf2 (ab92946) was purchased from Abcam. Secondary antibodies PE-IgG1 (clone A85-1), PE-IgG1 isotype control (clone MOPC-21) were purchased from BD Bioscience and Biolegend respectively. Detailed protocols for surface staining, intracellular staining have been described previously(44, 45). Flow cytometry analysis was performed with Cytek Aurora (Cytek Biosciences), and the FACS data were analyzed by using FlowJo software V10 (Tree star, Ashland, OR).

Histopathology

GVHD target organs including skin, liver, lung, small intestine and large intestine were harvested 21 days after BMT. The tissues were fixed in 10% formalin embedded in paraffin blocks, sectioned and stained with hematoxylin and eosin. Pathology scores of tissues were blindly evaluated by Dr. Chen Liu at Yale University as previously described (44-46).

Bioluminescent imaging

Recipient mice receiving luciferase expressing P815 or Raji cells were intraperitoneally injected with 200 μl luciferin purchased from Goldbio (St. Louis, MO), and then anesthetized using isoflurane for evaluating tumor growth in vivo by using IVIS Spectrum CT (PerkinElmer, Waltham, MA). Data were analyzed by using software purchased from PerkinElmer.

Real-time qPCR

T cells purified from syngeneic and allogenic BMT mice were extracted total RNA using Trizol reagent purchased from Thermos Fisher Scientific (Waltham, MA). RNAs were reversely transcribed into cDNA using reverse transcription kit purchased from BioRad

(Berkeley, CA). Quantitative real-time PCR was performed using SYBR Green (BioRad, CA). The mouse housekeeping gene, actin, was used as internal reference for data normalization. Fold changes in data figure 1B and 6C were calculated using △△Ct method. All primers are listed as follows (5'→3'):

Mouse Eif2ak3-F: ATGCCGGGGCTAAGTTGTAGA

Mouse Eif2ak3-R: AACGGATACGTCGTCTGGATA

Mouse Syvn1-F: CCAACATCTCCTGGCTCTTCCA

Mouse Syvn1-R: CAGGATGCTGTGATAAGCGTGG

Mouse Sel1l-F: GGAAGTGACATCGTACCTCAGAG

Mouse Sel1l-R: CTTGAACGCCTCTTCCGTAGAG

Mouse Erlec1-F: GCAGGAAGAGATACTGAGAGTGC

Mouse Erlec1-R: GGTTGTTCCAACAGTGAGCACTG

Mouse Atf4-F: GCCTGACTCTGCTGCTTA

Mouse Atf4-R: GCCTTACGGACCTCTTC

Mouse Os9-F: CATCGGCTGAAACGCTACCACA

Mouse Os9-R: CGGGTTCATCTACTCGGTCAATG

Mouse Ddit3-F: GGAGCTGGAAGCCTGGTATG

Mouse Ddit3-R: GGATGTGCGTGTGACCTCTG

Mouse Man1b1-F: AGTGGACTTCAGACAGCACGGT

Mouse Man1b1-R: GGATGTGCTTTGTCACTTCCTCC

Mouse Edem1-F: GCTGCGTATCAGAGCATCCAGA

Mouse Edem1-R: CAGCGAGTCAATCCAGGTGTTC

Mouse Edem2-F: GACCCTGTGTTTGAAGATGTGGC

Mouse Edem2-R: CACTTGCCAGTGAGCACATCGA

Mouse Edem3-F: CCACCACAAACCGAAGCATCTC

Mouse Edem3-R: GGTTCACGGATGCTCTGAGCAT

RNA-sequencing (RNA-seq)

Total RNA of T cells purified from WT and PERK cKO mice and stimulated with allogeneic APC or anti-CD3/CD28 were extracted using Trizol reagent (Thermos

Fisher Scientific, MA). The RNA concentration was evaluated by NanoDrop Microvolume Spectrophotometers (Thermos Fisher Scientific, Waltham, MA). RNA integrity was determined by running electrophoresis. Data were analyzed by using DESeq2, pheatmap and clusterProfiler packages using R and R studio software.

Immunoprecipitation and western blot

Immunoprecipitation was performed by adding specific antibodies into cell lysates for rotation overnight in 4 ℃. Next, protein A/G beads (Santa Cruz Biotechnology, Dallas, TX) were added for a rotation of 4-6 hrs in 4 ℃. The samples were then boiled with loading buffer for 10 min in 98 ℃ after washing 5 times with Thermo Scientific Pierce IP lysis buffer.

Cells were harvested and lysed using RIPA lysis buffer or IP lysis buffer supplemented with protease inhibitor cocktail (Sigma, US). Protein concentrations were measured by BCA Protein Assay Kit (Thermos Fisher Scientific, Waltham, MA) and equivalent proteins were subjected to SDS-PAGE gel, and then transferred to PVDF membrane. After blocking with 5% non-fat milk, the membrane was incubated with specific primary antibodies overnight at 4 ℃. Then, secondary antibodies were incubated for 1 hr at room temperature after washing 3 times. SuperSignal West Pico PLUS Chemiluminescent Substrate (Thermos Fisher Scientific, Waltham, MA) was used to visualize the immunoreactivity bands. Anti-mouse PERK (31292S), anti-mouse p-PERK (3179S), anti-human PERK (5683S), anti-mouse XBP-1s (12782S), anti-mouse/human GAPDH (2118S), and anti-mouse/human β-actin (8457T) antibodies were purchased from Cell Signaling Technology (Danvers, Massachusetts, US). Anti-mouse GADD153 (CHOP, sc-7351) was purchased from Santa Cruz (California, US). Anti-mouse/human SEL1L (ab78298), anti-mouse/human ERLEC1 (ab181166) antibodies were purchased from Abcam (Cambridge, UK).

Statistics

GraphPad Prism 9.0 was used to generate figures and statistics calculation. Survival comparison was analyzed by using Log-rank (Mantel-Cox) test. Both GVHD scores

and body weight loss comparisons were analyzed by using non-parametric Mann-Whitney U test. Multiple comparisons were determined by using a one-way or two-way ANOVA test. Comparisons between two groups were analyzed by using a two-tailed unpaired Student's *t* test. Data were shown as mean ± SD. $P < 0.05$ was considered as statistically significant (*$P < .05$, **$P < .01$, ***$P < .001$, ****$P < .0001$).

Study approval

Experimental protocols were approved by the IACUC of Medical College of Wisconsin (AUA00007677, AUA00007641).

Data availability

The values corresponding to all data points shown in graphs and values behind any reported means are available in the Supporting Data Values Excel file.

All data generated or analyzed during this study are included in the Fig.1–7 and Supplemental Fig. 1–16. Raw data will be uploaded online and provided by the corresponding author upon request. Raw data of RNA sequencing have been deposited in GEO database (GSE307389).

Author contributions

Q.C., H.-J.C., and X.-Z.Y. conceived and designed this project. Q.C., and H.-J.C. performed the experiments and analyzed data, Q.C. drafted the manuscript. Y. W. contributed to discussing BMT experiments and revising the manuscript. X.Y., A.P., L.T., M.H., D.F. contributed to the *in vivo* experiments. R.A. contributed to the human T cell *in vitro* experiments. X.-Z.Y. interpreted the data, revised the manuscript, and supervised the work.

Conflict-of-interest disclosure: The authors declare no competing financial interests.

Acknowledgments

The authors are grateful for the support provided by the Cancer Center Shared

Resource, Flow Cytometry Core and Laboratory Animal Research Department at Medical College of Wisconsin. We thank the Cancer Center Discovery & Developmental Therapeutics Research Program for supporting the travel award to ASH meeting.

This work was supported in part by NIH Grants including R01s CA258440, HL163584 and R21CA263140 as well as institutional start-up funds from the Cancer Center and Department of Microbiology & Immunology (X.-Z.Y.). It is subject to the NIH Public Access Policy. Through acceptance of this federal funding, NIH has been given a right to make this manuscript publicly available in PubMed Central upon the Official Date of Publication, as defined by NIH.

Address correspondence to: Xue-Zhong Yu, Department of Microbiology & Immunology, the Cancer Center, Medical College of Wisconsin, Milwaukee, WI, USA. Email: xuyu@mcw.edu.

References

1. Zeiser R, and Blazar BR. Acute Graft-versus-Host Disease - Biologic Process, Prevention, and Therapy. *N Engl J Med.* 2017;377(22):2167-79.
2. Zeiser R, and Teshima T. Nonclassical manifestations of acute GVHD. *Blood.* 2021;138(22):2165-72.
3. Haring E, Andrieux G, Uhl FM, Krausz M, Proietti M, Sauer B, et al. Therapeutic targeting of endoplasmic reticulum stress in acute graft-versus-host disease. *Haematologica.* 2022;107(7):1538-54.
4. Choi HJ, and Yu XZ. ER stress: an emerging regulator in GVHD development. *Front Immunol.* 2023;14:1212215.
5. Khateb A, and Ronai ZA. Unfolded Protein Response in Leukemia: From Basic Understanding to Therapeutic Opportunities. *Trends Cancer.* 2020;6(11):960-73.
6. Duan J, Matute JD, Unger LW, Hanley T, Schnell A, Lin X, et al. Endoplasmic reticulum stress in the intestinal epithelium initiates purine metabolite synthesis and promotes Th17 cell differentiation in the gut. *Immunity.* 2023;56(5):1115-31 e9.
7. Mandula JK, Chang S, Mohamed E, Jimenez R, Sierra-Mondragon RA, Chang DC, et al. Ablation of the endoplasmic reticulum stress kinase PERK induces paraptosis and type I interferon to promote anti-tumor T cell responses. *Cancer Cell.* 2022;40(10):1145-60 e9.
8. Song M, Sandoval TA, Chae CS, Chopra S, Tan C, Rutkowski MR, et al. IRE1alpha-XBP1 controls T cell function in ovarian cancer by regulating mitochondrial activity. *Nature.* 2018;562(7727):423-8.
9. Choi HJ, Wu Y, McDaniel Mims B, Pugel A, Tang CA, Tian L, et al. Endoplasmic Reticulum Stress Response Mediator IRE-1alpha Promotes Host Dendritic Cells in Graft-versus-Host Disease Development. *J*

Immunol. 2024;213(3):384-93.
10. Poncet AF, Bosteels V, Hoffmann E, Chehade S, Rennen S, Huot L, et al. The UPR sensor IRE1alpha promotes dendritic cell responses to control Toxoplasma gondii infection. *EMBO Rep.* 2021;22(3):e49617.
11. Cubillos-Ruiz JR, Silberman PC, Rutkowski MR, Chopra S, Perales-Puchalt A, Song M, et al. ER Stress Sensor XBP1 Controls Anti-tumor Immunity by Disrupting Dendritic Cell Homeostasis. *Cell.* 2015;161(7):1527-38.
12. Raines LN, Zhao H, Wang Y, Chen HY, Gallart-Ayala H, Hsueh PC, et al. PERK is a critical metabolic hub for immunosuppressive function in macrophages. *Nat Immunol.* 2022;23(3):431-45.
13. Mohamed E, Sierra RA, Trillo-Tinoco J, Cao Y, Innamarato P, Payne KK, et al. The Unfolded Protein Response Mediator PERK Governs Myeloid Cell-Driven Immunosuppression in Tumors through Inhibition of STING Signaling. *Immunity.* 2020;52(4):668-82 e7.
14. Hetz C, Chevet E, and Harding HP. Targeting the unfolded protein response in disease. *Nat Rev Drug Discov.* 2013;12(9):703-19.
15. Di Conza G, and Ho PC. ER Stress Responses: An Emerging Modulator for Innate Immunity. *Cells.* 2020;9(3).
16. Walter P, and Ron D. The unfolded protein response: from stress pathway to homeostatic regulation. *Science.* 2011;334(6059):1081-6.
17. Schutt SD, Wu Y, Tang CH, Bastian D, Nguyen H, Sofi MH, et al. Inhibition of the IRE-1alpha/XBP-1 pathway prevents chronic GVHD and preserves the GVL effect in mice. *Blood Adv.* 2018;2(4):414-27.
18. Szaruga M, Janssen DA, de Miguel C, Hodgson G, Fatalska A, Pitera AP, et al. Activation of the integrated stress response by inhibitors of its kinases. *Nat Commun.* 2023;14(1):5535.
19. Chintha C, Carlesso A, Gorman AM, Samali A, and Eriksson LA. Molecular modeling provides a structural basis for PERK inhibitor selectivity towards RIPK1. *RSC Adv.* 2019;10(1):367-75.
20. Cao Y, Trillo-Tinoco J, Sierra RA, Anadon C, Dai W, Mohamed E, et al. ER stress-induced mediator C/EBP homologous protein thwarts effector T cell activity in tumors through T-bet repression. *Nat Commun.* 2019;10(1):1280.
21. Hwang J, and Qi L. Quality Control in the Endoplasmic Reticulum: Crosstalk between ERAD and UPR pathways. *Trends Biochem Sci.* 2018;43(8):593-605.
22. Yao X, Wu Y, Xiao T, Zhao C, Gao F, Liu S, et al. T-cell-specific Sel1L deletion exacerbates EAE by promoting Th1/Th17-cell differentiation. *Mol Immunol.* 2022;149:13-26.
23. Gao Y, Li W, Wang Z, Zhang C, He Y, Liu X, et al. SEL1L preserves CD8(+) T-cell survival and homeostasis by fine-tuning PERK signaling and the IL-15 receptor-mediated mTORC1 axis. *Cell Mol Immunol.* 2023;20(10):1232-50.
24. Correa-Medero LO, Jankowski SE, Hong HS, Armas ND, Vijendra AI, Reynolds MB, et al. ER-associated degradation adapter Sel1L is required for CD8(+) T cell function and memory formation following acute viral infection. *Cell Rep.* 2024;43(5):114156.
25. Han J, Ma S, Gong H, Liu S, Lei L, Hu B, et al. Inhibition of Acute Graft-versus-Host Disease with Retention of Graft-versus-Tumor Effects by Dimethyl Fumarate. *Front Immunol.* 2017;8:1605.
26. Kusaczuk M. Tauroursodeoxycholate-Bile Acid with Chaperoning Activity: Molecular and Cellular Effects and Therapeutic Perspectives. *Cells.* 2019;8(12).
27. Khalaf K, Tornese P, Cocco A, and Albanese A. Tauroursodeoxycholic acid: a potential therapeutic tool in neurodegenerative diseases. *Transl Neurodegener.* 2022;11(1):33.
28. Arai Y, Choi B, Kim BJ, Rim W, Park S, Park H, et al. Tauroursodeoxycholic acid (TUDCA) counters osteoarthritis by regulating intracellular cholesterol levels and membrane fluidity of degenerated

chondrocytes. *Biomater Sci.* 2019;7(8):3178-89.
29. Fernandez-Sanchez L, Albertos-Arranz H, Ortuno-Lizaran I, Lax P, and Cuenca N. Neuroprotective Effects of Tauroursodeoxicholic Acid Involves Vascular and Glial Changes in Retinitis Pigmentosa Model. *Front Neuroanat.* 2022;16:858073.
30. Ajmal N, Bogart MC, Khan P, Max-Harry IM, and Nunemaker CS. Emerging Anti-Diabetic Drugs for Beta-Cell Protection in Type 1 Diabetes. *Cells.* 2023;12(11).
31. Bonnemain B. Pharmacokinetic and hemodynamic safety of two superparamagnetic agents, Endorem and Sinerem, in cirrhotic rats. *Acad Radiol.* 1998;5 Suppl 1:S151-3; discussion S6.
32. Smith AL, Andrews KL, Beckmann H, Bellon SF, Beltran PJ, Booker S, et al. Discovery of 1H-pyrazol-3(2H)-ones as potent and selective inhibitors of protein kinase R-like endoplasmic reticulum kinase (PERK). *J Med Chem.* 2015;58(3):1426-41.
33. Dey B, Yang YG, Preffer F, Shimizu A, Swenson K, Dombkowski D, and Sykes M. The fate of donor T-cell receptor transgenic T cells with known host antigen specificity in a graft-versus-host disease model. *Transplantation.* 1999;68(1):141-9.
34. Elfrink HL, Zwart R, Baas F, and Scheper W. Inhibition of endoplasmic reticulum associated degradation reduces endoplasmic reticulum stress and alters lysosomal morphology and distribution. *Mol Cells.* 2013;35(4):291-7.
35. Lin LL, Wang HH, Pederson B, Wei X, Torres M, Lu Y, et al. SEL1L-HRD1 interaction is required to form a functional HRD1 ERAD complex. *Nat Commun.* 2024;15(1):1440.
36. Mendes A, Gigan JP, Rodriguez Rodrigues C, Choteau SA, Sanseau D, Barros D, et al. Proteostasis in dendritic cells is controlled by the PERK signaling axis independently of ATF4. *Life Sci Alliance.* 2021;4(2).
37. Verfaillie T, Rubio N, Garg AD, Bultynck G, Rizzuto R, Decuypere JP, et al. PERK is required at the ER-mitochondrial contact sites to convey apoptosis after ROS-based ER stress. *Cell Death Differ.* 2012;19(11):1880-91.
38. Perea V, Cole C, Lebeau J, Dolina V, Baron KR, Madhavan A, et al. PERK signaling promotes mitochondrial elongation by remodeling membrane phosphatidic acid. *EMBO J.* 2023;42(15):e113908.
39. Shrestha N, Liu T, Ji Y, Reinert RB, Torres M, Li X, et al. Sel1L-Hrd1 ER-associated degradation maintains beta cell identity via TGF-beta signaling. *J Clin Invest.* 2020;130(7):3499-510.
40. Wang HH, Lin LL, Li ZJ, Wei X, Askander O, Cappuccio G, et al. Hypomorphic variants of SEL1L-HRD1 ER-associated degradation are associated with neurodevelopmental disorders. *J Clin Invest.* 2024;134(2).
41. Wang H, Rong X, Zhao G, Zhou Y, Xiao Y, Ma D, et al. The microbial metabolite trimethylamine N-oxide promotes antitumor immunity in triple-negative breast cancer. *Cell Metab.* 2022;34(4):581-94 e8.
42. Tang CH, Ranatunga S, Kriss CL, Cubitt CL, Tao J, Pinilla-Ibarz JA, et al. Inhibition of ER stress-associated IRE-1/XBP-1 pathway reduces leukemic cell survival. *J Clin Invest.* 2014;124(6):2585-98.
43. Sun S, Shi G, Han X, Francisco AB, Ji Y, Mendonca N, et al. Sel1L is indispensable for mammalian endoplasmic reticulum-associated degradation, endoplasmic reticulum homeostasis, and survival. *Proc Natl Acad Sci U S A.* 2014;111(5):E582-91.
44. Tian L, Wu Y, Choi HJ, Sui X, Li X, Sofi MH, et al. S1P/S1PR1 signaling differentially regulates the allogeneic response of CD4 and CD8 T cells by modulating mitochondrial fission. *Cell Mol Immunol.* 2022;19(11):1235-50.
45. Schutt SD, Wu Y, Kharel A, Bastian D, Choi HJ, Hanief Sofi M, et al. The druggable transcription factor Fli-1 regulates T cell immunity and tolerance in graft-versus-host disease. *J Clin Invest.* 2022;132(21).
46. Daenthanasanmak A, Iamsawat S, Chakraborty P, Nguyen HD, Bastian D, Liu C, et al. Targeting Sirt-1 controls GVHD by inhibiting T-cell allo-response and promoting Treg stability in mice. *Blood.* 2019;133(3):266-79.

751

Figure 1

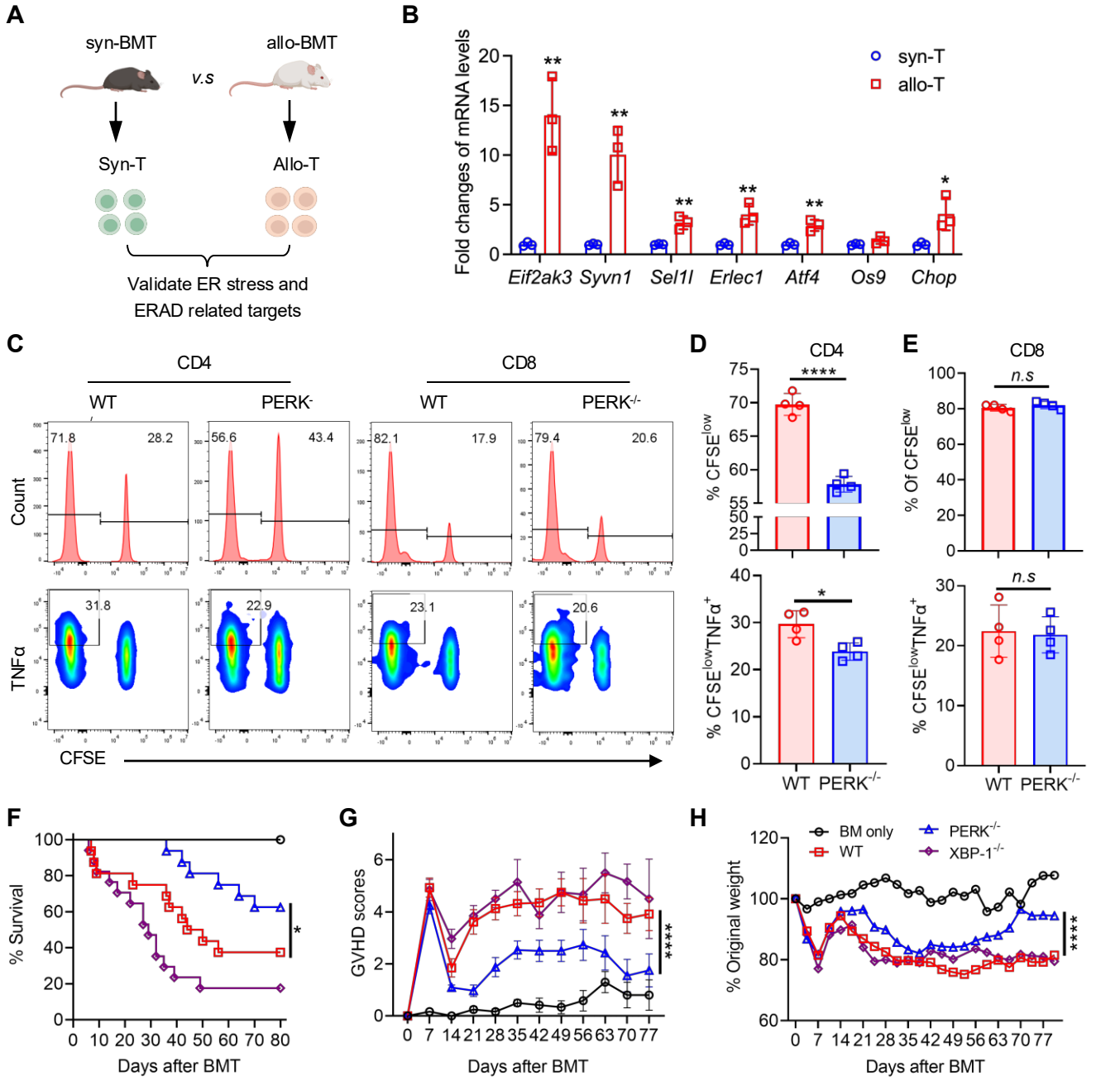

Figure 1. PERK but not XBP1 positively regulates T cell allogeneic responses and GVHD. (**A**) Lethally irradiated WT B6 (Ly5.1, syngeneic) and BALB/c (allogeneic) recipients were transferred with T cells (1.25 X 10^6) isolated from normal B6 (Ly5.2) donors plus BM cells (4 X 10^6) from Rag1-KO donors, n = 5 per group. (**B**) T cells were isolated from spleens of B6 (Ly5.1) and BALB/c recipients on day 14 after BMT and extracted total RNA. mRNA levels of *Eif2ak3*, *Syvin1*, *Sel1l*, *Erlec1*, *Atf4*, *Os9*, *Chop*, *Actin* were analyzed by Real-time qPCR. (**C**) T cells isolated from WT and PERK cKO mice were labeled with CFSE and stimulated with allogeneic APCs (TCD-splenocytes) from BDF1 mice for 4 days. The proliferation ($CFSE^{low}$) of $CD4^+$ or $CD8^+$ T cells and the levels of pro-inflammatory cytokines in $CD4^+$ or $CD8^+$ T cells were analyzed by flow cytometry. (**D**) Percentages of $CFSE^{low}CD4^+$ and $CFSE^{low}TNF\alpha^+CD4^+$ T cells among gated $H2K^{d-}CD4^+$ T cells are shown. (**E**) Percentages of $CFSE^{low}CD8^+$ and $CFSE^{low}TNF\alpha^+CD8^+$ T cells among gated $H2K^{d-}CD8^+$ T cells are shown. (**F-H**) Lethally irradiated BALB/c recipients were transferred with TCD-BM cells (5 X 10^6) alone or together with T cells (1.25 X 10^6) from WT B6 or PERK cKO or XBP1 cKO donors. Survival (**F**), GVHD scores (**G**), body weight (**H**) of BALB/c recipients were monitored through 80 days post-BMT, n = 5 for BM only, n = 16 for WT or PERK cKO or XBP1 cKO combined from 2 replicate experiments. Log-rank (Mantel-Cox) test (**F**) and non-parametric Mann-Whitney U test (**G**, **H**) were used to compare groups. Data in panels **B**, **D**, **E** are represented as mean ± standard error (SD), significance was determined using a two-tailed unpaired Student's *t* test. **P* < .05, ***P* < .01, ****P* < .001, *****P* < .0001. *n.s*, not significant.

Figure 2

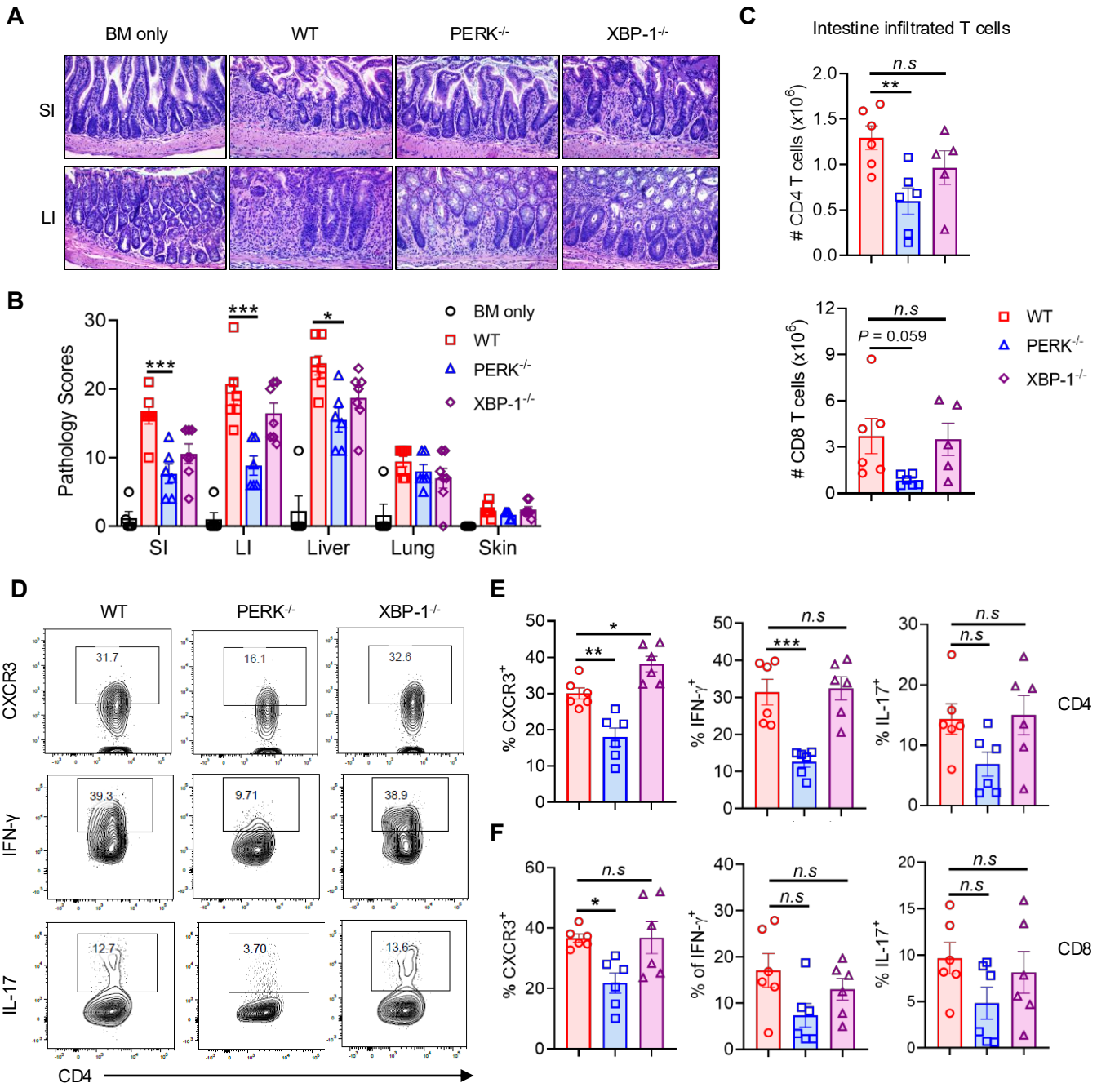

Figure 2. PERK-deficient T cells reduce the ability to induce GVHD and differentiate to Th1 and Th17 populations. Lethally irradiated BALB/c mice (900 cGy) were injected with TCD-BM cells (5 X 10^6) alone or together with T cells (1.25 X 10^6) isolated from WT B6, PERK cKO or XBP1 cKO donors, n = 5-7 per group. (**A**) Pathology of small intestine (SI) and large intestine (LI) of BALB/c recipients was analyzed on the tissues with HE staining. (**B**) Pathology scores of small and large intestines, liver, lung, skin are displayed. (**C**) Absolute number of infiltrated $CD4^+$ or $CD8^+$ T cells in intestine was analyzed on day 14 after BMT. (**D**) $CXCR3^+CD4^+$, $IFN\gamma^+CD4^+$, and $IL\text{-}17^+CD4^+$ T cells in intestine were analyzed by flow cytometry. (**E**) Percentages of $CXCR3^+CD4^+$, $IFN\gamma^+CD4^+$, and $IL\text{-}17^+CD4^+$ T cells among gated $H2K^{b+}CD4^+$ T cells are displayed. (**F**) Percentages of $CXCR3^+CD8^+$, $IFN\gamma^+CD8^+$, and $IL\text{-}17^+CD8^+$ T cells among gated $H2K^{b+}CD8^+$ T cells are displayed. Data in panels **B**, **C**, **E**, **F** are represented as mean ± SD, significance was determined using a one-way ANOVA test. *P < .05, **P < .01, ***P < .001.

Figure 3

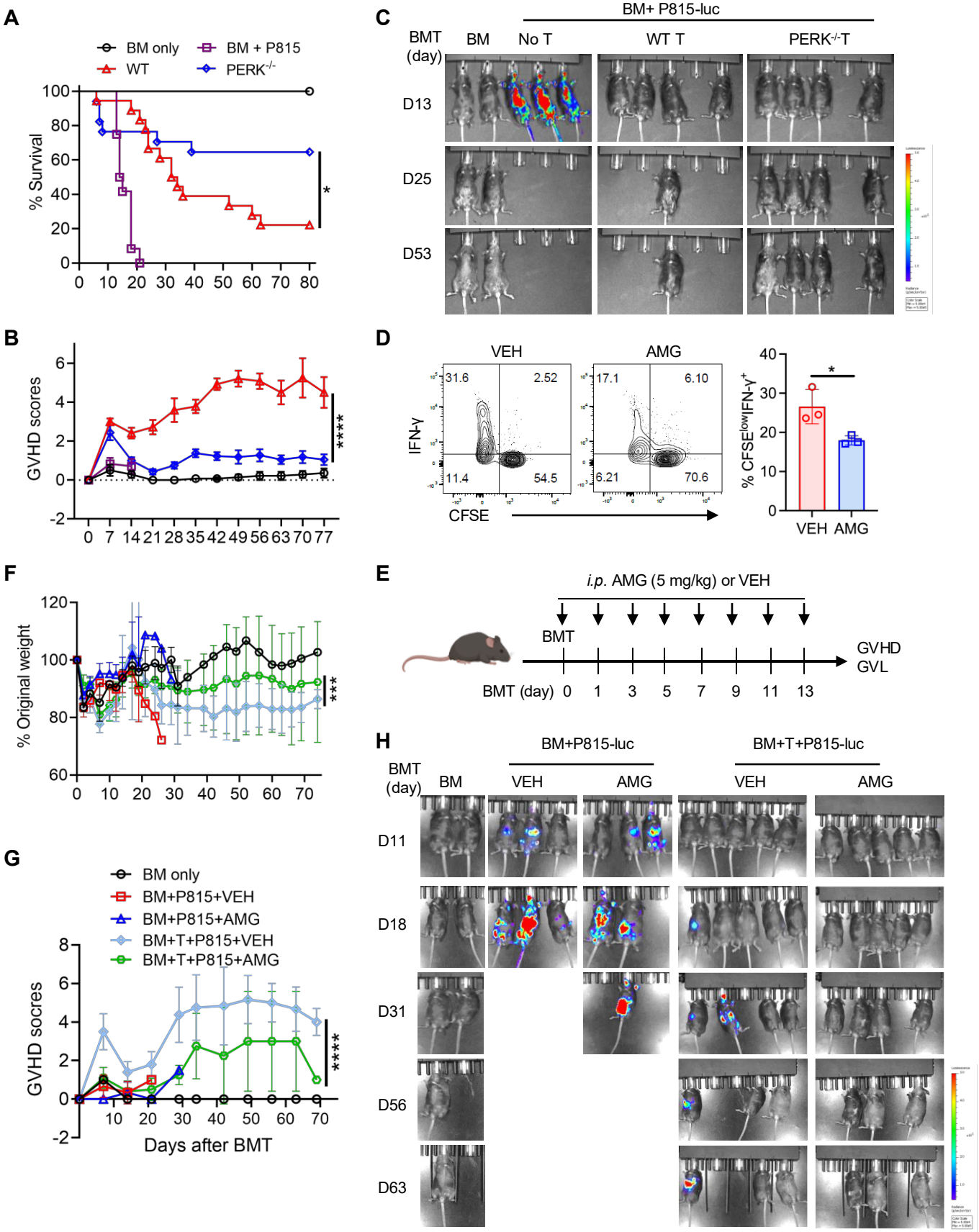
A
BM only
WT
BM + P815
PERK-/-
% Survival
*
B
GVHD scores
****
C
BM+ P815-luc
BMT (day)
BM
No T
WT T
PERK-/-T
D13
D25
D53
D
VEH
AMG
IFN-γ
CFSE
31.6
2.52
11.4
54.5
17.1
6.10
6.21
70.6
% CFSElowIFN-γ+
VEH
AMG
E
i.p. AMG (5 mg/kg) or VEH
BMT
GVHD
GVL
BMT (day) 0 1 3 5 7 9 11 13
F
% Original weight
***
G
BM only
BM+P815+VEH
BM+P815+AMG
BM+T+P815+VEH
BM+T+P815+AMG
GVHD socres
****
Days after BMT
H
BM+P815-luc
BM+T+P815-luc
BMT (day)
BM
VEH
AMG
VEH
AMG
D11
D18
D31
D56
D63

Figure 3. PERK deficiency in donor T cells does not impact their GVL activity while reducing ability to induce GVHD. (**A-C**) Lethally irradiated BDF1 mice were injected with TCD-BM cells (5 X 10^6) alone or together with luciferase-expressing P815 (P815-luc) cells (5000) with or without CD25-removed T cells (3 X 10^6) from WT or PERK cKO donors. Survival (**A**) and GVHD scores (**B**) were monitored through 80 days post-BMT. Tumor growth in BDF1 recipients was monitored using bioluminescent imaging (BLI) (**C**), n = 7 for BM only, n = 12 for BM with P815, n = 16-17 for WT or PERK cKO. (**D**) T cells isolated from WT B6 mice were labeled with CFSE, stimulated with allogeneic APCs from BALB/c mice for 4 days and treated with or without AMG44 (10 μM), $CFSE^{low}IFN\gamma^{+}CD4^{+}$ T cells was analyzed using flow cytometry. Percentage of $CFSE^{low}IFN\gamma^{+}CD4^{+}$ T cells among gated $H2K^{b+}CD4^{+}$ T cells is displayed. (**E-H**) Lethally irradiated BDF1 mice (1200 cGy) were injected with TCD-BM cells (5 X 10^6) alone or together with P815-luc cells (5000) and with or without CD25-removed T cells (3 X 10^6) from normal B6 mice. Vehicle or AMG44 (5 mg/kg) was intraperitoneally (*i.p*) injected into BDF1 recipients every other day for 2 weeks post-BMT (**E**). Body weight loss (**F**) and GVHD scores (**G**) were monitored through 80 days post-BMT. Tumor growth in BDF1 recipients was monitored using BLI (**H**), n = 2 for BM only, n = 3 for BM and P815 with VEH or AMG, n = 5 for BM+T+P815 with VEH or AMG. Log-rank (Mantel-Cox) test (**A**) and non-parametric Mann-Whitney U test (**B**, **F**, **G**) were used to compare groups. Data in panel **D** are represented as mean ± SD with biological replicates, significance was determined using a two-tailed unpaired Student's *t* test. **P* < .05.

Figure 4

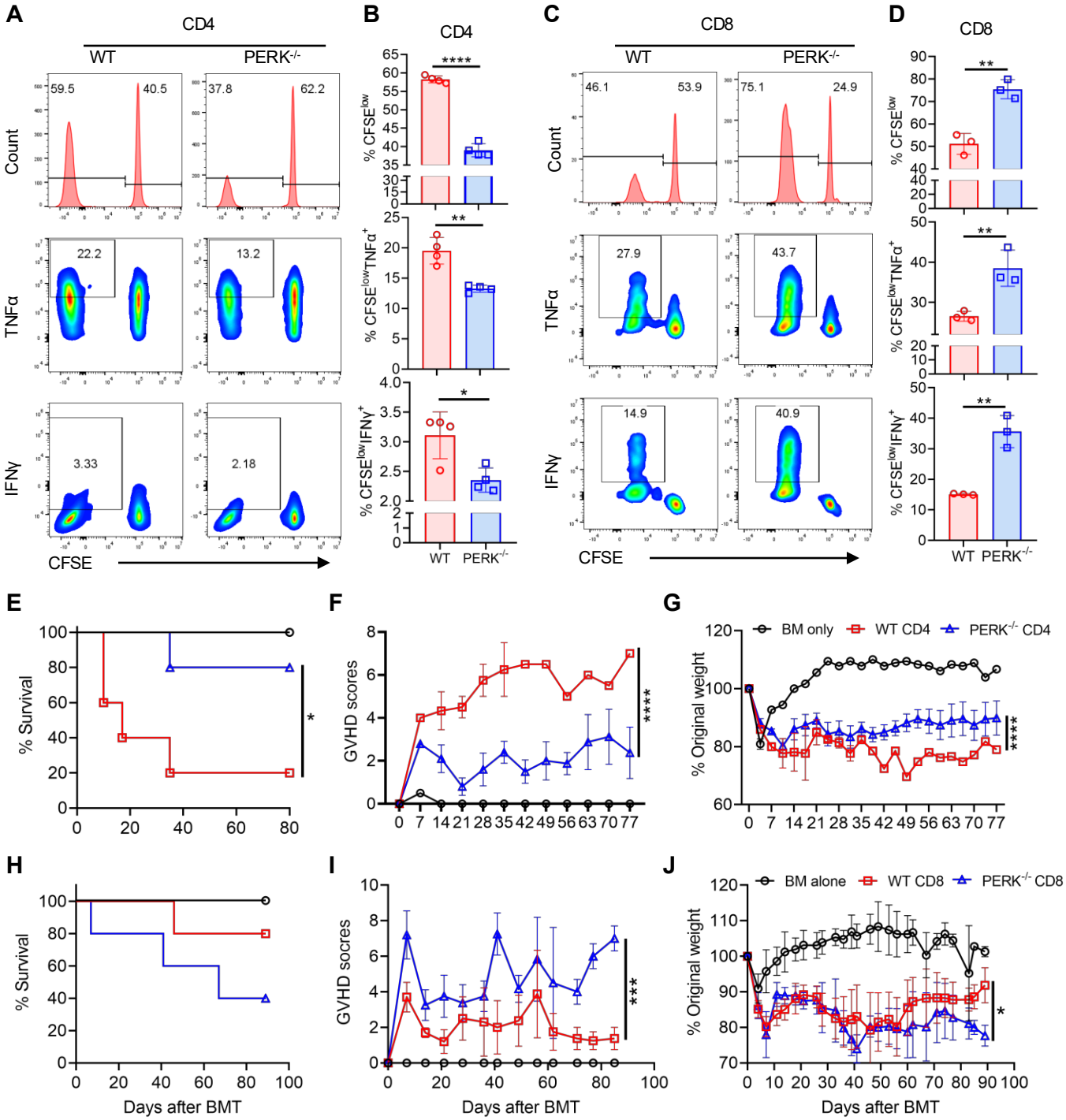

Figure 4. PERK differentially regulates CD4 and CD8 T-cell responses to alloantigens. (**A-B**) $CD4^+$ T cells isolated from WT or PERK cKO mice were stimulated with allogeneic APCs from BDF1 mice for 4 days, proliferation ($CFSE^{low}$) of $CD4^+$ T cells, and levels of pro-inflammatory cytokines (TNFα, IFNγ) in $CD4^+$ T cells were analyzed using flow cytometry (**A**). Percentages of $CFSE^{low}CD4^+$, $CFSE^{low}TNFα^+CD4^+$, $CFSE^{low}IFNγ^+CD4^+$ T cells among gated $H2K^dCD4^+$ T cells are shown (**B**). (**C-D**) $CD8^+$ T cells isolated from WT or PERK cKO mice were stimulated with allogeneic APCs from BDF1 mice for 4 days, proliferation ($CFSE^{low}$) of $CD8^+$ T cells, and levels of pro-inflammatory cytokines (TNFα, IFNγ) in $CD8^+$ T cells were analyzed by flow cytometry (**C**). Percentages of $CFSE^{low}CD8^+$, $CFSE^{low}TNFα^+CD8^+$, $CFSE^{low}IFNγ^+CD8^+$ T cells among gated $H2K^dCD8^+$ T cells are shown (**D**). (**E-G**) Lethally irradiated BALB/c recipients were injected with TCD-BM (5 X 10^6) cells alone or together with $CD4^+$ T cells (1.25 X 10^6) from WT C57BL/6 or PERK cKO donors. Survival (**E**), GVHD scores (**F**), body weight (**G**) of BALB/c recipients were monitored through 80 days post-BMT. n = 5 per BMT group. (**H-J**) Lethally irradiated BALB/c recipients (900 cGy) were injected with TCD-BM cells (5 X 10^6) alone or along with $CD8^+$ T cells (2.5 X 10^6) from WT B6 or PERK cKO donors and CD25-removed $CD4^+$ T cells (0.5 X 10^6) from WT B6 mice. Survival (**H**), GVHD scores (**I**), body weight (**J**) of BALB/c recipients were monitored through 80 days post-BMT, n = 5 per BMT group. Log-rank (Mantel-Cox) test (**E**, **H**) and non-parametric Mann-Whitney U test (**F**, **G**, **I**, **J**) were used to compare groups. Data in panels **B**, **D** are represented as mean ± SD with biological replicates, significance was determined using a two-tailed unpaired Student's *t* test. **P* < .05, ***P* < .01, ****P* < .001, *****P* < .0001.

Figure 5

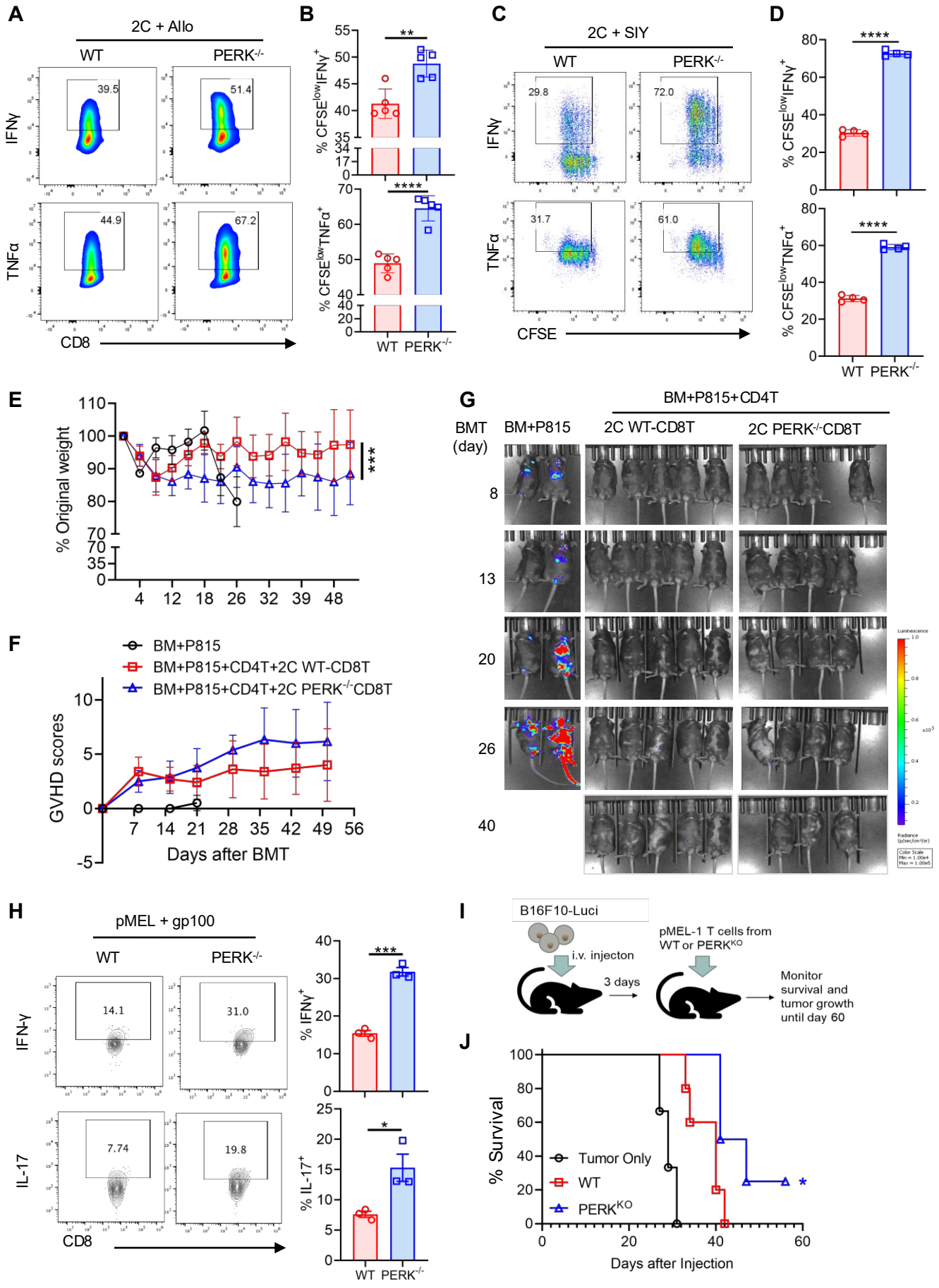
A
2C + Allo
WT
PERK-/-
IFNγ
TNFα
CD8
39.5
51.4
44.9
67.2
B
% CFSE^low IFNγ+
% CFSE^low TNFα+
WT PERK-/-
C
2C + SIY
29.8
72.0
31.7
61.0
CFSE
D
E
% Original weight
Days after BMT
F
BM+P815
BM+P815+CD4T+2C WT-CD8T
BM+P815+CD4T+2C PERK-/-CD8T
GVHD scores
G
BM+P815+CD4T
BMT (day)
BM+P815
2C WT-CD8T
2C PERK-/-CD8T
H
pMEL + gp100
IFN-γ
IL-17
14.1
31.0
7.74
19.8
% IFNγ+
% IL-17+
I
B16F10-Luci
i.v. injecton
3 days
pMEL-1 T cells from WT or PERKKO
Monitor survival and tumor growth until day 60
J
% Survival
Tumor Only
WT
PERKKO
Days after Injection

Figure 5. PERK inhibits CD8 T-cell responses. (**A-B**) $CD8^+$ T cells isolated from 2C transgenic WT or PERK cKO mice were labeled with CFSE and stimulated with allogeneic APCs from BDF1 mice for 4 days, the levels of pro-inflammatory cytokines (IFNγ, TNFα) in $CD8^+$ T cells were analyzed by flow cytometry (**A**). Percentages of $CFSE^{low}IFN\gamma^+CD8^+$ and $CFSE^{low}TNF\alpha^+CD8^+$ T cells among gated $H2K^{d-}CD8^+$ T cells are shown (**B**). (**C-D**) $CD8^+$ T cells isolated from 2C transgenic WT or PERK cKO mice were labeled with CFSE and stimulated with SIY peptides (10 nM) together with syngeneic APC isolated from B6 mice (Ly5.1) for 3 days, levels of pro-inflammatory cytokines (IFNγ, TNFα) in $CD8^+$ T cells were analyzed using flow cytometry (**C**). Percentages of $CFSE^{low}IFN\gamma^+CD8^+$ T cells and $CFSE^{low}TNF\alpha^+CD8^+$ T cells among gated $CD45.1^-CD8^+$ T cells are shown (**D**). (**E-G**) Lethally irradiated BDF1 mice (1200 cGy) were given TCD-BM cells (5 X 10^6) alone or along with P815-luc cells (5000) with or without CD25-removed T cells (3 X 10^6) purified from 2C transgenic WT or PERK cKO donors. Body weight loss (**E**) and GVHD scores (**F**) were monitored through 80 days post-BMT. Tumor growth in BDF1 recipients was monitored via BLI (**G**), n = 5 per BMT group. (**H**) $CD8^+$ T cells isolated from pMEL transgenic WT or PERK cKO mice were stimulated with gp100 peptides together with syngeneic APC isolated from B6 mice (Ly5.1) for 3 days, the levels of IFNγ and IL-17 in $CD8^+$ T cells were analyzed by flow cytometry, percentages of $IFN\gamma^+CD8^+$ and $IL\text{-}17^+CD8^+$ T cells among gated $CD45.1^-CD8^+$ T cells are shown. (**I-J**) Lethally irradiated BDF1 mice (1100 cGy) were injected with TCD-BM cells (5 X 10^6) along with B16F10-luc cells with or without CD25-removed T cells (3 X 10^6) purified from pMEL transgenic WT or PERK cKO donors, n = 3 for tumor only, n = 5-6 for WT or PERK cKO (**I**). Survival (**J**) was monitored through 60 days post-BMT. Log-rank (Mantel-Cox) test (**J**) and non-parametric Mann-Whitney U test (**E**, **F**) were used to compare groups. Data in panels **B**, **D**, **H** are represented as mean ± SD with biological replicate, significance was determined using a two-tailed unpaired Student's *t* test. **P* < .05, ***P* < .01, ****P* < .001, *****P* < .0001.

Figure 6

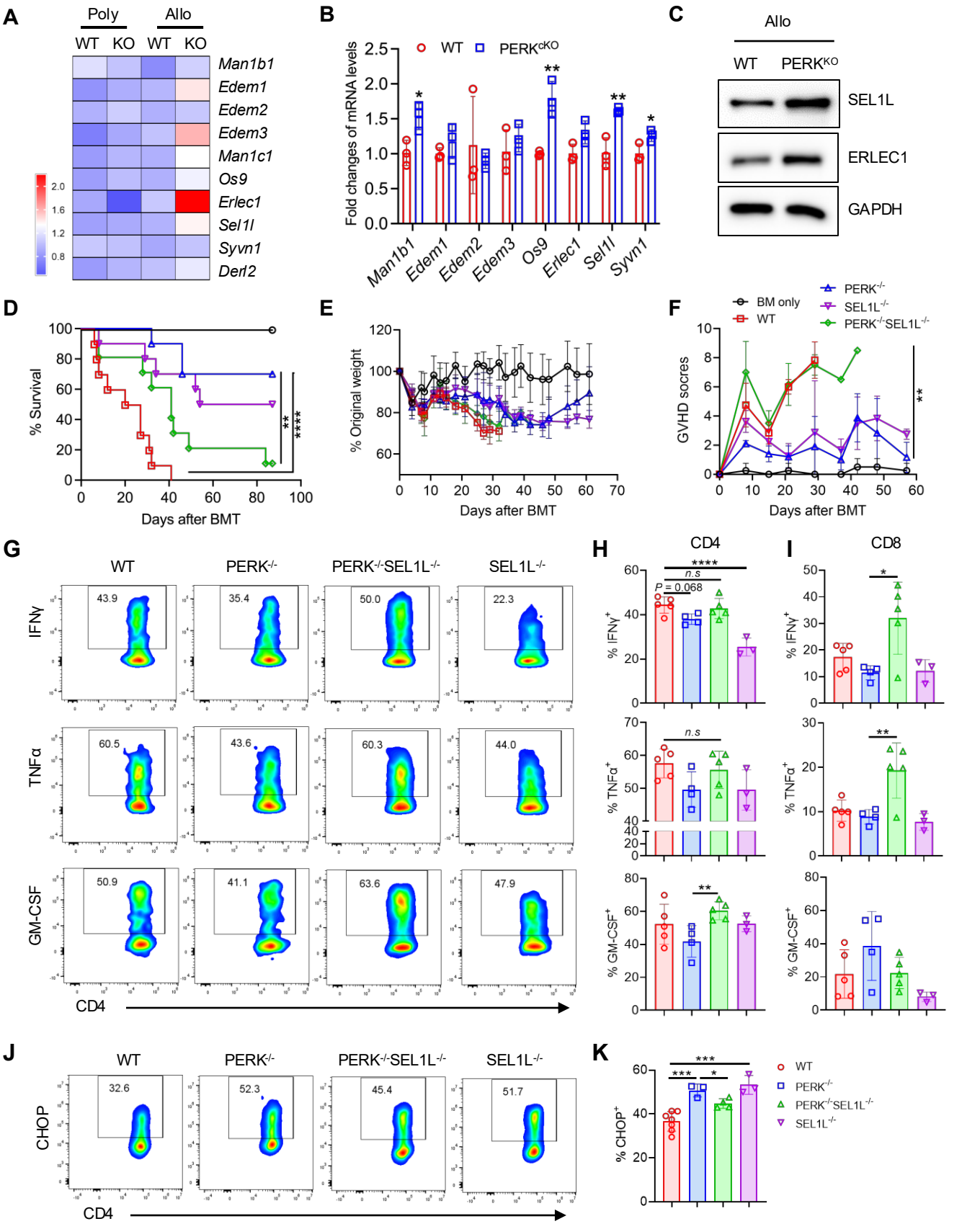
A
Poly
Allo
WT KO WT KO
Man1b1
Edem1
Edem2
Edem3
Man1c1
Os9
Erlec1
Sel1l
Syvn1
Derl2
2.0
1.6
1.2
0.8
B
WT
PERKcKO
Fold changes of mRNA levels
Man1b1
Edem1
Edem2
Edem3
Os9
Erlec1
Sel1l
Syvn1
C
Allo
WT
PERKKO
SEL1L
ERLEC1
GAPDH
D
% Survival
Days after BMT
E
% Original weight
Days after BMT
F
BM only
WT
PERK-/-
SEL1L-/-
PERK-/-SEL1L-/-
GVHD socres
Days after BMT
G
WT
PERK-/-
PERK-/-SEL1L-/-
SEL1L-/-
IFNγ
TNFα
GM-CSF
43.9
35.4
50.0
22.3
60.5
43.6
60.3
44.0
50.9
41.1
63.6
47.9
CD4
H
CD4
% IFNγ+
% TNFα+
% GM-CSF+
n.s
P = 0.068
I
CD8
J
WT
PERK-/-
PERK-/-SEL1L-/-
SEL1L-/-
CHOP
32.6
52.3
45.4
51.7
CD4
K
% CHOP+
WT
PERK-/-
PERK-/-SEL1L-/-
SEL1L-/-

Figure 6. PERK regulates T-cell allogeneic responses through ERAD. (**A**) T cells isolated from WT or PERK cKO mice were stimulated with anti-CD3 (2 μg/ml) and anti-CD28 (2 μg/ml) for 3 days or allogeneic APCs for 4 days, then T cells were isolated and performed RNA sequencing. Differentially expressed ERAD-associated genes were shown in the heat map. (**B-C**) T cells from WT or PERK cKO mice were stimulated by allogeneic APCs for 4 days, mRNA levels of indicated ERAD-associated genes in allogeneic T cells were analyzed by Real-time qPCR (**B**). (**C**) Protein levels of SEL1L, ERLEC1, β-actin indicated were evaluated using antibodies against SEL1L, ERLEC1, β-actin by western blot. (**D-F**) Lethally irradiated BALB/c recipients were injected with TCD-BM (5 X 10^6) cells alone or together with T cells (1.25 X 10^6) from WT, PERK cKO, SEL1L cKO, or PERK-SEL1L double KO (dKO) donors. Survival (**D**), body weight (**E**) GVHD scores (**F**) of BALB/c recipients were monitored through 80 days post-BMT, n = 9-10 combined from two replicate experiments. (**G-K**) Lethally irradiated BALB/c recipients were injected with BM cells (5 X 10^6) isolated from Rag1 KO mice along with T cells (1.25 X 10^6) purified from WT, PERK cKO, SEL1L cKO, or PERK-SEL1L dKO donors. (**G**) The levels of IFNγ, TNFα, GM-CSF in donor $CD4^+$ or $CD8^+$ T cells of livers from the recipients were analyzed by flow cytometry. (**H**) Percentages of $IFN\gamma^+CD4^+$, $TNF\alpha^+CD4^+$, and $GM\text{-}CSF^+CD4^+$ T cells among gated $H2K^{b+}CD4^+$ T cells are shown. (**I**) Percentages of $IFN\gamma^+CD8^+$, $TNF\alpha^+CD8^+$, $GM\text{-}CSF^+CD8^+$ T cells among gated $H2K^{b+}CD8^+$ T cells are shown. (**J**) The levels of CHOP in donor $CD4^+$ T cells were analyzed by flow cytometry. (**K**) Mean fluorescent intensity (MFI) of CHOP among gated $H2K^{b+}CD4^+$ T cells is displayed. Log-rank (Mantel-Cox) test (**D**) and non-parametric Mann-Whitney U test (**E**, **F**) were used to compare groups. Data in panel **B** are represented as mean ± SD, significance was determined using a two-tailed unpaired Student's *t* test. Data in panels **H**, **I**, **K** are represented as mean ± SD, significance was determined using a one-way ANOVA test. **P* < .05, ***P* < .01, ****P* < .001, *****P* < .0001.

Figure 7

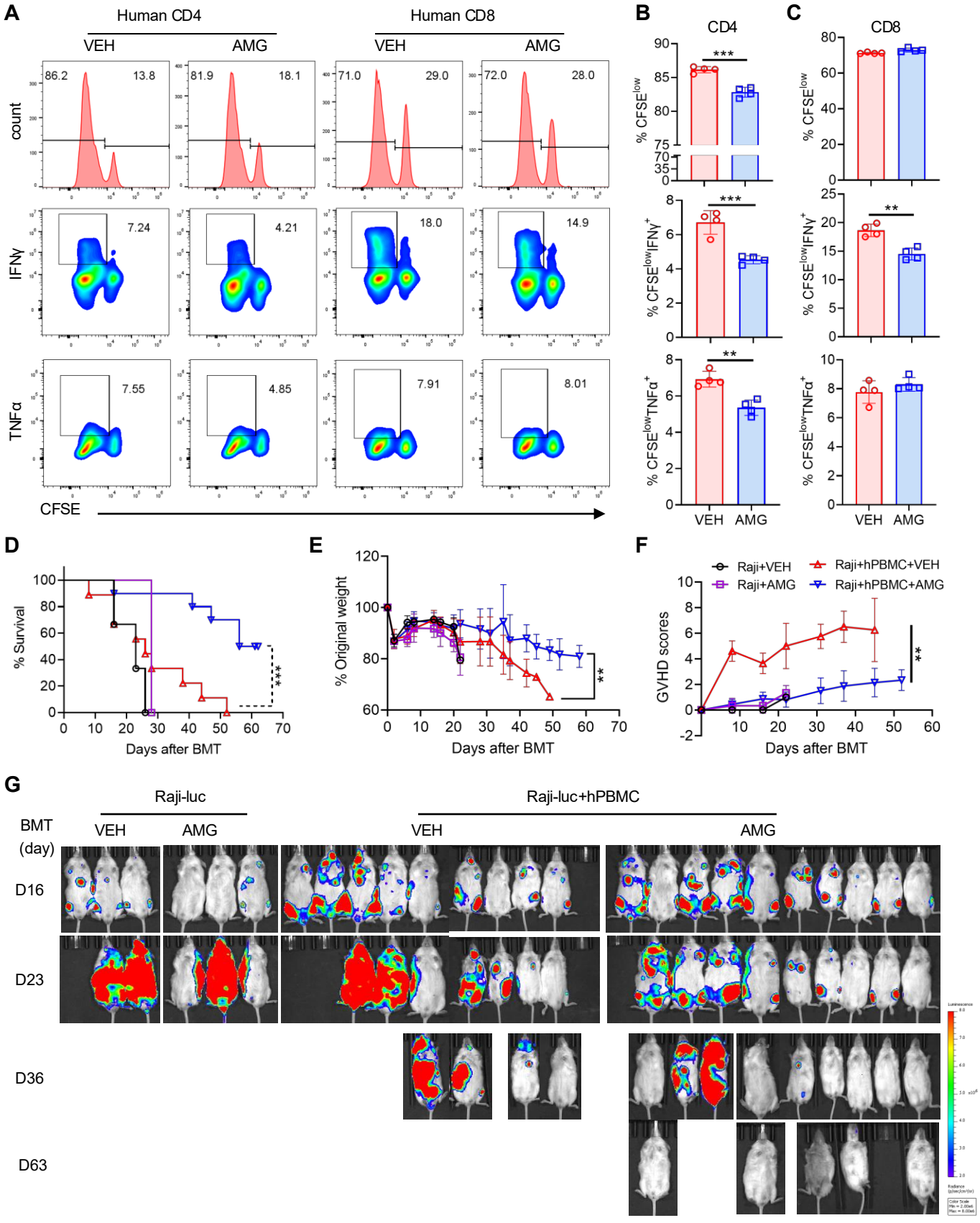
A
Human CD4
Human CD8
VEH
AMG
VEH
AMG
count
86.2
13.8
81.9
18.1
71.0
29.0
72.0
28.0
IFNγ
7.24
4.21
18.0
14.9
TNFα
7.55
4.85
7.91
8.01
CFSE
B
CD4
% CFSE^low
% CFSE^low IFNγ+
% CFSE^low TNFα+
C
CD8
% CFSE^low
% CFSE^low IFNγ+
% CFSE^low TNFα+
VEH
AMG
D
% Survival
Days after BMT
E
% Original weight
Days after BMT
F
Raji+VEH
Raji+AMG
Raji+hPBMC+VEH
Raji+hPBMC+AMG
GVHD scores
Days after BMT
G
Raji-luc
Raji-luc+hPBMC
BMT (day)
VEH
AMG
VEH
AMG
D16
D23
D36
D63

Figure 7. Inhibition of PERK reduces GVHD induced by human T cells while maintaining GVL activity. (**A-C**) T cells were isolated from human HLA-A2$^-$PBMCs, labeled with CFSE and stimulated with allogeneic HLA-A2$^+$APCs (TCD-PBMCs), proliferation and production of IFNγ, TNFα, Granzyme B (GZMB) of donor CD4$^+$ and CD8$^+$ T cells were analyzed by flow cytometry (**A**). Percentages of CFSE^{low}CD4$^+$, IFNγ$^+$CD4$^+$, TNFα$^+$CD4$^+$, and GZMB$^+$CD4$^+$ T cells among gated HLA-A2$^-$CD4$^+$ T cells are shown (**B**). Percentages of CFSE^{low}CD8$^+$, IFNγ$^+$CD8$^+$, TNFα$^+$CD8$^+$, and GZMB$^+$CD8$^+$ T cells among gated HLA-A2$^-$CD8$^+$ T cells are shown (**C**). (**D-G**) Sub lethally irradiated NSG mice were injected with Raji-Luc cells along with or without human PBMCs (8 X 10^6). Recipient mice were treated with vehicle or AMG44 (5 mg/kg) every other day from day 0 to 14. Survival (**D**), body weight loss (**E**), and GVHD scores (**F**) were monitored through 60 days after BMT, n = 3 for Raji with VEH or AMG, n = 9-10 for Raji and PBMC with VEH or AMG combined from 2 replicate experiments. Tumor growth in NSG recipients was monitored via BLI (**G**). Log-rank (Mantel-Cox) test (**D**) and non-parametric Mann-Whitney U test (**E**, **F**) were used to compare groups. Data in panels **B**, **C** are represented as mean ± SD with biological replicates, significance was determined using a two-tailed unpaired Student's *t* test. **P* < .05, ***P* < .01, ****P* < .001, *****P* < .0001.